Immunogenicity and protection efficacy of self-amplifying and circular mRNA vaccines for SARS-CoV-2

Oinam Ningthemmani Singh[1], Umang Berry[1], Garima Joshi[2], Tejeswara Rao Asuru[2], Kannan Chandrasekar[1], Sriram Narayanan[3], Puneet Srivastava[1], Mahima Tiwari[1], Souvick Chattopadhyay[4], Farha Mehdi[4], Bhisma Narayan Panda[5], Debasis Nayak[6], Shailendra Mani[1], Tripti Shrivastava[1], Gaurav Batra[4], C.T. Ranjith-Kumar[3], Prasenjit Guchhait[2], Milan Surjit[1*]

[1]Centre for Virus research, therapeutics and vaccines, Translational Health Science and Technology Institute, National Capital Region Biotech Science Cluster, Faridabad, Haryana, India.

[2]Regional Centre for Biotechnology, National Capital Region Biotech Science Cluster, Faridabad, Haryana, India.

[3]University School of Biotechnology, Guru Gobind Singh Indraprastha University, New Delhi, India.

[4]Centre for Biodesign, Translational Health Science and Technology Institute, National Capital Region Biotech Science Cluster, Faridabad, Haryana, India.

[5]Experimental animal facility, Translational Health Science and Technology Institute, National Capital Region Biotech Science Cluster, Faridabad, Haryana, India.

[6]Department of Biological Science, Indian Institute of Science Education and Research (IISER) Bhopal IISER, Bhopal, India.

Correspondence: milan@thsti.res.in

Running title: SARS-CoV-2 SAM & circ-RNA vaccine comparison

Abstract

Recent studies have demonstrated safety and reliability of messenger RNA (mRNA) vaccines for human use. Conventionally, mRNA vaccines use linear or self-amplifying mRNA (SAM), the latter considered to be superior. However, COVID-19 SAM vaccines showed limited success. Further, Circular mRNA (Circ-RNA) vaccines against the SARS-CoV-2, Ebola and monkey pox proved its efficacy. Circ-RNAs are highly stable, do not induce innate immune pathway RNA sensors nor require any extracellular protein for their function. Here, we compared the efficacy of SAM- and Circ-RNA vaccines using the SARS-CoV-2-RBD (receptor binding domain) antigen. Both SAM-RBD and Circ-RBD induced a comparable anti-RBD IgG titer and virus-neutralization titer. However, the latter induced a significantly higher memory T-cell response. Circ-RBD formulation was stable in refrigerator, induced a durable neutralizing antibody response, protected mice from COVID-19-like pathology and a bivalent vaccine containing the Circ-RNA-RBD of SARS-CoV-2-Delta and Omicron variants potently neutralized both viruses. These finding demonstrate the overall superiority of the Circ-RNA over the SAM vaccine technology and provides the proof of concept for developing bivalent Circ-RNA vaccines against emerging variants of SARS-CoV-2.

Introduction

Although messenger RNA (mRNA) vaccines have been researched for more than two decades, its proof of success in real-life was witnessed for the first time during the COVID-19 pandemic. Comirnaty, the first FDA (United States food and drug administration)-approved COVID-19 vaccine (developed by Pfizer-BioNTech) and Spikevax (COVID-19 vaccine developed by Moderna), both mRNA vaccines, were pivotal in controlling the COVID-19. Since then, there is considerable momentum to develop mRNA vaccines against multiple pathogens, allergic diseases and cancer[1-6]. Advances in mRNA delivery technology, *in vitro* transcription technology and reduction in the cost of production have improved the overall yield, stability, efficacy and economic viability of the mRNA vaccine, thereby positioning it as the preferred option for vaccine development[7]. Both linear mRNA (such as Comirnaty and Spikevax) and self-amplifying mRNA (SAM) (such as Gemcovac)-based vaccines have been approved for use in human[1,2,8]. More recently, several independent studies have demonstrated the efficacy of circular mRNA (Circ-RNA) vaccines[9-12].

Linear mRNA-encoding the vaccine antigen is generally small in size (compared to the SAM), contain a methyl-guanosine cap analog at the 5'-end, poly A-tailed at the 3'-end and the antigen-encoding sequence is flanked by untranslated regions (UTR) at both sides. A major challenge of linear mRNA-based vaccines is low stability of the input mRNA. Stability of the linear mRNAs are increased by incorporating pseudo-uridine or N6-Methyladenosine (m6A) into the sequence[13,14]. SAM vaccines are generally based on engineered genome of alphaviruses such as the Venezuela Equine Encephalitis virus (VEEV), Semliki Forest Virus (SFV) or Sindbis virus (SINV)[15]. Here, the viral structural protein-encoding sequence is replaced with the sequence of the vaccine antigen so that non-structural proteins of the virus enables replication the viral genome without production of infectious progeny virions. Thus, SAM vaccines should produce the required quantity of antigen for a prolonged period with less amount of the input RNA (compared to the linear mRNA), leading to a stronger and more durable immune response[16]. However, use of viral replication machinery for amplifying the input RNA has certain disadvantages such as: size of the SAM RNA is considerably longer as it contains the sequence to express viral non-structural proteins; viral RNA-dependent RNA polymerase, which is required for replication of the SAM RNA has low fidelity, increasing the possibility of introducing mutation(s) in the antigen-encoding sequence; pre-existing anti-vector immunity remains a concern; generation of dsRNA during the replication of SAM might activate host defence machinery leading to degradation of SAM; possibility of uncontrolled and excessive replication of SAM due to mutations in the non-structural proteins cannot be ruled out. Notably, one of the SAM vaccines (COVAC1) failed to induce 100% seroconversion while another SAM vaccine (ARCT154) showed a very good response in phase I clinical

107 trials[17,18]. Gemcovac (Gennova), a commercially available SAM vaccine, also shows very good
108 protection efficacy in clinical trials[8].
109 Circular RNAs (Circ-RNA) are covalently closed single-stranded RNA without free 5'- and 3'-
110 ends. It is produced naturally through back-splicing, which involves the connection of the 3'-
111 end of an exon to the 5'- end of another exon, creating a close loop RNA. The circular structure
112 provides resistance to most of the RNases except RNase A, RNase T1 and RNase T2, thus
113 significantly increasing their half-life compared to linear mRNAs. Endogenous Circ-RNAs act
114 as miRNA sponges to regulate various cellular processes by binding to nucleic acids and
115 proteins, thereby modulating transcription and cellular signalling pathways[19]. Circ-RNAs do
116 not induce the cellular innate immune pathway RNA sensors[20,21]. Recent reports have
117 demonstrated the ability of engineered Circ-RNAs to express the vaccine antigens using
118 internal ribosomal entry site (IRES)-mediated translation, thereby eliminating the requirement
119 of capping of the 5'-end of the mRNA[22,9]. Circ-RNA-based vaccines against the Severe acute
120 respiratory syndrome-coronavirus-2 (SARS-CoV-2) and Monkey pox has been shown to
121 induce potent immune response and protect the animals from challenge with the respective
122 viruses[9,12]. Notably, in the case of SARS-CoV-2, Circ-RNA immunization produced a higher
123 T_H1 biased humoral immune response and a higher neutralizing to binding antibody ratio than
124 its mRNA counterpart, supporting its protection efficacy and superior potential for evading the
125 antibody-dependent enhancement (ADE)[9].
126 SARS-CoV-2, the causative agent of the coronavirus-induced disease-19 (COVID-19), is
127 responsible for the worst global pandemic of the 21st century. So far approximately 771 million
128 COVID-19 cases and 7 million deaths have been reported globally
129 (https://data.who.int/dashboards/covid19). The viral genome shows high mutation rate,
130 leading to emergence of multiple variants, some of which, such as the B.1.617.2 (Delta) and
131 the Omicron B.1.1.529 (BA.1) variants pose serious health issues[23,24]. Omicron B.1.1.529
132 (BA.1) became the most dominant circulating strain with 22 subvariants accounting for 87%
133 of infections. Omicron strain dominated the previous variant of concern (VOC) in 2022 and
134 carries the most significant number of mutations than the previous VOC, with 37 mutations
135 within its spike protein. 15 mutations at the RBD region covering almost all the critical mutation
136 sites, such as K417N, S477N, T478K, E484A and N501Y make more transmissible and
137 immune evasion to pre-existing immunity. Previous non-Omicron infection or vaccination has
138 little protection against the Omicron variant[25-27]. The Omicron sub-variants, including the
139 BA.4/5 and XBB, continue to emerge, with total immune escaping potential to the previous
140 vaccination. Few studies have shown the broader protective efficacy of bivalent mRNA and
141 nanoparticle vaccines composed of a mixture of antigens from the SARS-CoV-2-Beta and
142 Delta or Delta and Omicron variants[28-30]. Despite development of several vaccines against the

143 SARS-CoV-2, there is limited access to vaccines globally and there is scope for improving the
144 efficacy and duration of protection offered by the vaccines.
145 Being the viral outer surface protein, spike protein of the SARS-CoV-2 is the main target for
146 vaccine development. The receptor binding domain (RBD) of the spike protein, which accounts
147 for one-fifth of the total protein, produced over 90% of the neutralizing antibody in infected
148 patients[31]. There are no reports of antibody dependent enhancement (ADE) by vaccines
149 based on the full length spike protein of the SARS-CoV-2. However, possibility of ADE
150 induction by the spike protein of emerging SARS-CoV-2 variants cannot be ruled out.
151 Therefore, RBD would be the best target for developing SARS-CoV-2 vaccines.
152 In the present study, we compared the immunogenicity and virus neutralization potential of
153 the Circ-RNA and SAM-RNA vaccine candidates using the SARS-CoV-2-RBD as the vaccine
154 antigen. Although both Circ-RBD (Circ-RNA backbone) and SAM-RBD (SAM-RNA backbone)
155 elicited comparable humoral and neutralizing antibody response, the former induced a
156 significantly higher T_H1-biased cellular immune response and protected mice from challenge
157 with the SARS-CoV-2. Further, Circ-RBD vaccine was stable in refrigerator, induced a durable
158 neutralizing antibody response and a bivalent vaccine formulation encoding the RBD of Delta
159 (Circ-RBD^{Del}) and Omicron (Circ-RBD^{Omi}) variants induced high cross-neutralizing antibody
160 response against both variants, confirming the protective efficacy of the Circ-RNA vaccines.
161 Significance of these findings in designing better mRNA vaccines based on circular RNA
162 technology is discussed.
163

164 **Results**

165 **Production and characterization of the SARS-CoV-2 SAM-RBD and Circ-RBD**
166 **vaccine formulations**

167 Self-splicing property of the Anabaena intron (Group 1) was utilized to generate the
168 Circ-RNA encoding the SARS-CoV-2-RBD (Wuhan isolate) fused to the CD5 signal
169 sequence (SS) and the sequence encoding the trimerization motif of bacteriophage
170 T4 fibritin (foldon) at the N- and C- terminus, respectively. The fusion protein was
171 translated under control of a Coxsackie virus B3 (CVB3) internal ribosome entry site,
172 as reported earlier[22]. A bacteriophage T7 promoter sequence was placed upstream of
173 the anabaena intron sequence at the 5'-end to enable *in-vitro* transcription-mediated
174 synthesis of Circ-RBD. A Semliki Forest virus (SFV) replicon was engineered to
175 produce the self-amplifying RNA encoding the SARS-CoV-2-RBD (SAM-RBD). RBD-
176 encoding sequence fused to the CD5 signal sequence and T4 fibritin foldon sequence at
177 its 5'- and 3'-ends was inserted into the SFV replicon. *In-vitro* transcription was carried out

178 using the SP6 polymerase, followed by Cap1-capping of the RNA. Sized integrity of the RNAs
179 were verified by spectrophotometry and formaldehyde-agarose gel electrophoresis. Expected
180 sized of the RNAs were observed (Figure 1A). An aliquot of the RNAs were treated with the
181 RNase R to check their circularization status. SAM-RBD was completely digested by RNase
182 R treatment whereas majority of Circ-RBD was resistant, confirming its circularization
183 (Figure1A). Next, RNA was encapsulated into the lipid-nanoparticle (LNP) by microfluidic
184 mixing and the diameter of the resulting RNA-LNP formulation was measured. The average
185 diameter of the SAM-RBD-LNP and the Circ-RBD-LNP was found to be 140 and 136nm,
186 respectively (Figure 1B). Average polydispersity index (PDI) of the SAM-RBD-LNP and the
187 Circ-RBD-LNP was 0.06 and 0.04, respectively (Figure 1C). LNP encapsulation and stability
188 of the SAM-RBD and the Circ-RBD RNA in the LNP complex was verified by resolving the
189 RNA-LNP complex with or without treatment with Triton X-100 (disrupts the LNP). No RNA
190 was visible in the SAM-RBD-LNP and the Circ-RBD-LNP complex-containing samples (Figure
191 1D). Treatment of the sample with Triton X-100 results in detection of the SAM-RBD and Circ-
192 RBD (Figure 1D). No difference was observed in the quality of the SAM-RBD and Circ-RBD
193 RNA before and after LNP encapsulation (Figure 1D). Percentage LNP encapsulation of the
194 SAM-RBD and Circ-RBD RNA was quantified using Ribogreen. 98.3% and 95.9% of SAM-
195 RBD and Circ-RBD RNA, respectively, was LNP-encapsulated (Figure 1E). Scanning electron
196 microscopy analysis of the SAM-RBD-LNP and Circ-RBD-LNP complexes revealed spherical
197 structure with average diameter of 136nm and 149nm respectively (Figure 1F). Next, SAM-
198 RBD-LNP and Circ-RBD-LNP complexes were transfected into HEK293T cells to detect the
199 expression of RBD. Western Blot analysis of the whole cell extract using the anti-RBD antibody
200 confirmed expression of the RBD protein (Figure 1G, upper panel). An aliquot of the whole
201 cell extract was probed using the anti-GAPDH antibody to check equal loading of the sample
202 (Figure 1G, lower panel). Secretion of RBD protein into the culture medium was checked by
203 anti-RBD western blot of the culture medium collected from the cells used in the above
204 experiment (shown in Figure 1G). RBD was detected in the culture medium as 2 distinct
205 bands, likely representing the glycosylated variants of the same protein (Figure 1H). Aliquots
206 of the same sample were resolved in non-reduced state to check trimerization status of the
207 RBD protein. As expected, anti-RBD western blot detected a band of approximately 100kDa
208 in the non-reduced samples, indicative of RBD-trimer (Figure 1I). Possible activation of the
209 innate immune pathways by the SAM-RBD and Circ-RBD RNAs were checked by RT-qPCR
210 analysis of IFN-β, RIG-I, OASL, PKR and OAS1 genes. None of these genes were induced
211 by either of the RNAs (Figure 1J). As a positive control, cells were transfected with poly I:C in
212 parallel, which is known to induce the cellular antiviral response pathway (Figure 1J).
213 Collectively, these results confirmed LNP encapsulation of SAM-RBD and Circ-RBD RNA and
214 expression of RBD protein trimer by both the RNAs. Importantly, western blot analysis also

215 demonstrated that approximately same amount of RBD was produced by both the SAM-RBD
216 and the Circ-RBD. Therefore, our experimental condition was suitable to compare the immune
217 response induced by the SAM-RBD and the Circ-RBD.
218
219 **SAM-RBD and Circ-RBD induced significant T_H1-biased humoral and cellular immune**
220 **response in mice**
221 To select the injection route and the optimal RNA dose, Balb/c mice were immunized via
222 intradermal (ID) or intramuscular (IM) route with freshly prepared vaccine formulation
223 containing 25μg Circ-RBD RNA. Two weeks later, immunization was repeated and blood was
224 collected after four weeks (day 28). Both ID and IM routes showed similar anti-RBD IgG titer
225 (average values: $6X10^5$ and $1X10^6$, respectively) and virus neutralization titer (average NT_{50}=
226 $1.7X10^3$ and $1.9X10^3$, respectively) (Figures S1A and B). ID immunization route was selected
227 for all subsequent experiments. Next, mice were injected with 5, 10 and 25μg of Circ-RBD-
228 RNA containing vaccine formulations in a two-dose immunization schedule as described
229 above. Measurement of anti-RBD IgG titer revealed average values to be $2.2X10^4$, $2.8X10^5$,
230 $6X10^5$ and average virus neutralization titer (NT_{50}) was found to be $0.5X10^3$, $1.5X10^3$, $0.8 X10^3$,
231 in 5, 10 and 20μg RNA containing formulations, respectively (Figures S1C and S1D). There
232 was no significant difference in values obtained between all 3 doses, hence 10μg RNA
233 containing formulation was selected for all subsequent experiments.
234 In order to evaluate the immune response generated by the Circ-RBD and SAM-RBD, 10μg
235 of each RNA containing vaccine formulation was intradermally injected into Balb/c mice in two
236 dose immunization schedules at two-week interval, followed by collection of blood and spleen
237 samples for analysis of different immune parameters (Figure 2A). Significant level of anti-RBD
238 IgM was detected in the sera of mice immunized with both SAM-RBD and Circ-RBD RNA
239 (Figure 2B). Importantly, no significant difference was observed in the level of IgM between
240 SAM-RBD and Circ-RBD immunized mice (Figure 2B). Measurement of anti-RBD IgG titer
241 and virus neutralization titer (NT_{50}) in the sera collected on day 28 from SAM-RBD and Circ-
242 RBD immunized mice revealed the average values to be $2.8X10^5$ and $3.2X10^6$ (anti-RBD-IgG
243 titer) and $1X10^3$ and $1.5X10^3$ (NT_{50}), respectively (Figures 2C and 2D). IgG-isotyping of
244 aliquots of the same sera showed comparable values between SAM-RBD and Circ-RBD
245 groups (Figures 2E-2G). The ratio of anti-RBD (IgG2a+IgG2b) to IgG1 was found to be 1.9
246 and 1.8, respectively, indicating a T_H1 response (Figure 2H). Next, splenocytes from these
247 mice were cultured *in vitro* and induced with overlapping peptide pool corresponding to the
248 RBD region, followed by selection of $CD4^+$ and $CD8^+$ T cells and quantification of intracellular
249 T_H1 (IFN-γ, TNF-α) and T_H2 (IL-4) cytokines. Both $CD4^+$ and $CD8^+$ T cells of mice immunized
250 with Circ-RBD induced significant IFN-γ and TNF-α response (Figures 2I-2L). A significant

251 IFN-γ and TNF-α response was observed in $CD4^+$ and $CD8^+$ T cells, respectively, in SAM-
252 RBD immunized mice (Figures 2I and 2L). An increased trend was observed in IFN-γ and
253 TNF-α level in $CD8^+$ and $CD4^+$ T cells, respectively, in SAM-RBD immunized mice although it
254 was not statistically significant (Figures 2J and 2K). There were no significant changes in IL-4
255 response in both SAM-RBD and Circ-RBD immunized mice, indicating that both vaccine
256 formulations induced T_H1-biased T-cell immune response (Figures 2M and 2N).
257 Representative FACS plots are shown (Figure S2). Collectively, these results demonstrate
258 that both SAM-RBD and Circ-RBD induced a robust and comparable humoral immune
259 response, however, the latter induced a better T_H1-biased cell-mediated immune response.

260 **Circ-RBD vaccine formulation is stable at four degrees centigrade and induces a**
261 **durable immune response in both female and male mice**

262 We evaluated the stability of the Circ-RBD vaccine formulation upon prolonged storage (up to
263 4 weeks) in the refrigerator (4^0C). The Circ-RBD vaccine formulations were stored in aliquots
264 in the refrigerator for 2 or 4 weeks, followed by evaluation of their physical and functional
265 characteristics. No change in particle diameter, polydispersity index and percent RNA
266 encapsulation was observed between the samples stored for 2 and 4 weeks, compared to the
267 freshly prepared sample (0 week) (Figures 3A-3C). Mice were injected with aliquots of the
268 same samples in a two-dose immunization schedule (as described above), followed by
269 collection of blood on the 28th day. There was no difference in the anti-RBD IgG titer and the
270 virus neutralization titer (NT_{50}) between freshly prepared and two weeks-stored samples (IgG
271 titer=$2.8X10^5$ and $4X10^5$, NT_{50}=$1.7X10^3$ and $1.3X10^3$ respectively) (Figures 3D and 3E). There
272 was approximately one log drop in the anti-RBD IgG titer and a 1.5 log drop in the virus
273 neutralization titer in the samples stored for 4 weeks at 4^0C (IgG titer=$0.6X10^5$,
274 NT_{50}=$0.04X10^3$) (Figures 3D and 3E).

275 Next, durability of the immune response and influence of gender on the immune response
276 elicited by the Circ-RBD was evaluated by immunizing male and female mice with the Circ-
277 RBD vaccine formulation in a two-dose immunization schedule (day 1 and day 14), followed
278 by measurement of the anti-RBD IgG titer and the virus neutralization titer (NT_{50}) up to 9
279 months. Both the anti-RBD IgG titer and the virus neutralization titer (NT_{50}) were measured in
280 the mice sera at 1, 3 and 9 months post-first immunization. There was no drop in the anti-RBD
281 IgG titer or the virus neutralization titer (NT_{50}) after 9 months of immunization, with reference
282 to the samples collected after one month of the first immunization (Figures 3G and 3H). Both
283 male and female mice induced a similar level of the anti-RBD IgG titer and the virus
284 neutralization titer (NT_{50}) (Figures 3G and 3H). Collectively, these results demonstrated that
285 Circ-RBD vaccine formulation is stable in standard refrigeration condition and induced a highly
286 durable neutralizing antibody response in both male and female mice.

287

288 **Immunization with the Circ-RBD vaccine protects mice from the SARS-CoV-2 infection**
289 **and prevents COVID-19 associated pathological changes**

290 A mouse model of intranasal SAR-CoV-2 infection was established as described[32]. The
291 experimental plan is illustrated (Figure 4A). Mice were injected with freshly prepared Circ-RBD
292 vaccine formulation on day 0 and day 14, intranasally transduced with replication deficient
293 adenovirus expressing the human angiotensin converting enzyme 2 (Ad5CMV-hACE2,
294 denoted as hACE2 hereafter) on day 28, followed by infection with 10^5 PFU of SARS-CoV-2
295 (Wuhan isolate) on day 33. Body weight of the animals were measured every day, blood was
296 collected prior to infection and 4 days after infection (day 37), animals were sacrificed on day
297 37 and bronchoalveolar lavage (BAL) and lung tissue were collected for analysis. As expected,
298 SARS-CoV-2 infection led to loss of body weight in the placebo group (Figure 4B). There was
299 equal loss of weight in the Circ-RBD immunized group on the day one post-infection (Figure
300 4B). However, no further weight loss was observed in the immunized group on second and
301 third days and animals starting gaining weight by fourth day post-infection, suggesting that
302 vaccinated mice were more resistant to SARS-CoV-2 infection induced weight loss (Figure
303 4B). Anti-RBD IgG titer was much higher in the Circ-RBD immunized SARS-CoV-2 infected
304 mice compared to the placebo group infected with SARS-CoV-2 on day 37 (10^6 vs 10^3) (Figure
305 4C). No virus or viral RNA was detected in the lungs and BAL of Circ-RBD immunized mice
306 whereas significant quantity of virus and viral RNA was detected in the placebo group on day
307 37 (the 5th day of infection) (Figures 4D, 4E, 4F). Further, morphology and histopathology
308 analysis of lung tissue of placebo and Circ-RBD immunized showed a striking difference
309 between the two groups. Multiple lesions were visible in the placebo group lungs whereas
310 Circ-RBD lungs appeared normal (Figure 4G). Histopathology analysis of the hematoxylin and
311 eosin-stained lung tissue sections showed pneumonia and inflammatory cells infiltration
312 (Figure 4H). Quantification of lung infiltration score and percent hematoxylin-stained area in
313 the slides from placebo and Circ-RBD immunized mice revealed high lung infiltration score
314 and higher hematoxylin-stained area in the placebo group (Figures 4I, 4J). Further, expression
315 of the proinflammatory cytokines and IFN-γ were significantly higher in the lungs of the placebo
316 group compared to the Circ-RBD immunized group (Figure 4K). Taken together, these results
317 confirmed that immunization with Circ-RBD protected the mice against the SARS-CoV-2.

318 In order to further evaluate the protection efficacy of the Circ-RBD vaccine, we wanted to
319 establish another mouse model of the SARS-CoV-2 infection that produces a more severe
320 disease phenotype. Intra-tracheal administration of the hACE2 has been shown to express
321 the hACE2 in mouse lungs within 5 days of transduction[33]. We hypothesized that increased
322 hACE2 expression in the lungs will permit more pronounced SARS-CoV-2 infection in the
323 lungs, leading to a more severe disease phenotype. To test the hypothesis, mice were

transduced with the hACE2 via intra-tracheal administration, followed by intranasal infection with the SARS-CoV-2. This model displayed a more severe pathogenic effect, including lethality. The experimental plan is summarized (Figure 5A). Next, the animals were immunized twice at 2 weeks intervals followed by intratracheal transduction of the hACE2 (on day 28). 10^5 PFU of the SARS-CoV-2 (Wuhan) was intranasally administered after 5 days and disease parameters were followed up for next three weeks (day 54). In the placebo group, there was a marked reduction in the body weight from the 2nd day of infection up to the 10th day, after which there was a gradual increase in the body weight up to the 21st day (Figure 5B). In the case of Circ-RBD immunized group, weight loss was observed between the 2nd to 5th day post-infection after which the animals gained weight, indicating that Circ-RBD vaccine protected the animals from progressing to severe disease pathology (Figure 5B). The weight profile of each mouse is represented (Figure S3A). Placebo group animals appeared sick, displayed hunchback posture, barely moved and importantly, three animals died during the observation period (one animal each died on day 36, 38 and 40) (Figure 5C). The remaining four animals started improving from day 47 (two weeks post-infection) onwards. Notably, Circ-RBD immunized animals were almost normal throughout the observation period.

Anti-RBD IgG titer was measured in the placebo and Circ-RBD immunized group on day 40 and 47 (one- and two-weeks post-infection, respectively). There was no significant anti-RBD IgG in the placebo group after one week of infection and an average titer of 10^5 was observed after two weeks of infection (Figure 5D). Circ-RBD immunized group showed anti-RBD IgG titer of 10^6 in the samples collected after one- and two-weeks of infection (Figure 5D). Estimation of viral load and viral RNA levels in the lung revealed higher viral load (10^3 PFU/mg of lung) and higher viral RNA levels (approximately ten-fold higher) in the lungs of placebo group (samples collected on day 40) compared to the Circ-RBD immunized group (Figures 5E, 5F). Both viral load and viral RNA levels were significantly less in the placebo group samples collected on day 47, which inversely correlated with the anti-RBD IgG titer observed at the same time point (Figures 5E, 5F). Placebo group also showed higher expression of proinflammatory cytokines and IFN-γ in the lung compared to that of the Circ-RBD immunized group (Figure 5G). Morphology and histopathology analysis of lung tissue of placebo group showed multiple lesions, pneumonia and infiltration of inflammatory cells whereas Circ-RBD immunized lungs appeared closed to normal in the samples collected on day 54 (Figures 5H, 5I). A similar profile was observed in the lung samples collected on day 47 (Figures S3B, S3C). Lung morphology and histopathology of both placebo and Circ-RBD immunized mice, collected on day 40 showed few lesions and inflammatory cells (Figures S3D, S3E). Quantification of lung inflammatory score and percentage of hematoxylin-stained area in the slides further confirmed the above observation (Figures 5J, 5K). Collectively, SARS-CoV-2

360 challenged studies in both the mice models confirmed the functional ability of the Circ-RBD
361 vaccine in protecting the animals against COVID-19.
362
363 **A bivalent SARS-CoV-2 Circ-RBD vaccine induces robust immune response and**
364 **efficiently neutralizes both the Delta and the Omicron BA.1 variant viruses**
365 Recent reports on bivalent mRNA vaccines and nanoparticle vaccine demonstrate their
366 efficacy in conferring broad spectrum immunity against the SARS-CoV-2 variants of concern[29-
367 31]. Feasibility of using the Circ-RNA vaccine technology for developing a bivalent vaccine was
368 tested by evaluating the immunogenicity and virus neutralization potential of a vaccine
369 formulation containing 1:1 mixture of the Circ-RNAs encoding the RBD of the Delta (Circ-
370 RBD^{Del}) and the Omicron BA.1 (Circ-RBD^{Omi}) variants of the SARS-CoV-2. Sequence
371 encoding the RBD region of the Delta and the Omicron variants of the SARS-CoV-2 were
372 inserted into the Circ-RNA backbone vector in place of the RBD (Wuhan) sequence so that
373 both RBD^{Del} and RBD^{Omi} are fused in-frame with the CD5 secretory signal and foldon
374 sequence at their N- and C- terminus, respectively. Expression and secretion of the RBD^{Del}
375 and RBD^{Omi} were verified by western blot analysis of the whole cell lysate and the culture
376 medium of the HEK239T cells transfected with the Circ-RBD^{Del}-LNP and Circ-RBD^{Omi}-LNP
377 formulations. Anti-RBD western blot reveled that both Circ-RBD^{Del} and Circ-RBD^{Omi} were
378 expressed in the HEK239T cells and secreted to the culture medium (Figures 6A, upper panel,
379 6B, upper and middle panel). Secretion of the Circ-RBD^{Omi} was not as efficient as that of the
380 Delta and the Wuhan variants as the ratio of protein in intracellular to culture medium was
381 much higher in the RBD^{Omi} (Figure 6B, middle panel). GAPDH level was measured in aliquots
382 of the same samples to monitor equal loading (Figures 6A, 6B, lower panel). Mice were
383 injected with vaccine formulations containing 10μg of Circ-RBD^{Wuhan}, Circ-RBD^{Del}, Circ-RBD^{Omi}
384 or 1:1 mixture of 5μg Circ-RBD^{Del} and 5ug Circ-RBD^{Omi} in a two-dose immunization schedule
385 at two weeks intervals, as described earlier, followed by collection of blood on day 28 and
386 estimation of the anti-RBD IgG titer and the virus neutralization titer. Mice immunized with the
387 vaccines containing the Circ-RBD^{Wuhan}, Circ-RBD^{Del} and Circ-$RBD^{Del+Omi}$ produced an anti-
388 RBD IgG titer of approximately 10^6 against the SARS-CoV-2 Wuhan and Delta variants
389 whereas it was $0.3x10^5$, $0.6x10^5$ and $0.6x10^5$, respectively in case of the Omicron variant
390 (Figures 6C, 6D, 6E). In contrast, the Circ-RBD^{Omi} vaccine induced an average anti-RBD IgG
391 titer of $1.2x10^5$ against the SARS-CoV-2 Wuhan and Delta variants and $1.8x10^5$ against the
392 Omicron variant (Figures 6C, 6D, 6E). The virus neutralization titer (NT_{50}) of the sera showed
393 a pattern broadly similar to that of the anti-RBD IgG titer. As observed earlier, NT_{50} of sera
394 from the Circ-RBD^{Wuhan} immunized group against the Wuhan variant was $3.5x10^3$ (Figure 6F).
395 Sera from the Circ-RBD^{Del} and Circ-$RBD^{Del+Omi}$ showed approximately similar NT_{50} as that of

396 the Circ-RBD^{Wuhan} (Figure 6F). However, NT_{50} of sera from the Circ-RBD^{Omi} immunized mice
397 against the Wuhan variant was found to be $0.2x10^3$, which is in line with the data on its anti-
398 RBD IgG titer against the same variant (Figure 6F). NT_{50} of sera from the Circ-RBD^{Del} and the
399 Circ-RBD$^{Del+Omi}$ immunized mice against the SARS-CoV-2 Delta variant was found to be
400 $8.1x10^3$ and $8.8x10^3$, respectively, indicating that the virus neutralization efficacy of the
401 bivalent vaccine was similar to its monovalent counterparts (Figure 6G). Sera from the Circ-
402 RBD^{Wuhan} immunized mice was almost as efficient as sera from the Circ-RBD^{Del} immunized
403 mice in neutralizing the SARS-CoV-2 Delta variant (NT_{50}= $1.7x10^3$) (Figure 6G). However,
404 sera from the Circ-RBD^{Omi} immunized mice were significantly less efficient in neutralizing the
405 SARS-CoV-2 Delta variant than that of the Circ-RBD^{Wuhan}, Circ-RBD^{Del} and Circ-RBD$^{Del+Omi}$
406 immunized mice (Figure 6G). Sera from the Circ-RBD^{Omi} and Circ-RBD$^{Del+Omi}$ immunized mice
407 showed an NT_{50} of $8.1x10^3$ and $2.3x10^3$, respectively, against the SARS-CoV-2 Omicron BA.1
408 variant, indicating that bivalent vaccine was equally effective as its monovalent (Circ-RBD^{Omi})
409 counterpart (Figure 6H). NT_{50} of sera from the Circ-RBD^{Del} and the Circ-RBD^{Wuhan} immunized
410 mice against the Omicron BA.1 variant were found to be $0.3x10^3$ and $0.06x10^3$ respectively,
411 suggesting that they were less efficient in neutralizing the Omicron BA.1 virus (Figure 6H).
412 Collectively, these data demonstrate that the bivalent Circ-RBD vaccine produces potent
413 neutralizing antibodies against the Delta and the Omicron BA.1 variants of the SARS-CoV-2.
414

415 **Discussion**

416 With the success of the COVID-19 mRNA vaccines, immunogenicity and protective efficacy
417 of a number of vaccine candidates based on linear mRNAs, self-amplifying mRNAs and
418 circular mRNAs have been evaluated in multiple independent studies. Given their ability to
419 replicate inside the host, SAM RNAs express the antigen for a longer duration with lesser
420 amount of the input RNA. Analogous to the SAM-RNA, Circ-RNAs also offer the advantage of
421 expression of the antigen for a longer duration with lesser amount of the input RNA, owing to
422 their higher stability. On top of that, Circ-RNA vaccines do not produce any additional
423 exogenous protein in the target cells, lack open 5'- and 3'-ends and do not produce double
424 strand RNA (dsRNA) in the target cell, all of which are potential unwanted features in the SAM
425 vaccine. Therefore, Circ-RNA vaccines appear to be more promising than the linear mRNA
426 and SAM vaccines. Comparison between linear mRNA and Circ-RNA vaccines have
427 demonstrated the superiority of the later[9]. However, there are no report on comparison of the
428 protective efficacy between the Circ-RNA and the SAM vaccines. Here, we compared the
429 efficacy of the Circ-RNA and the SAM vaccines by measuring their immunogenicity and virus
430 neutralization potential using the SARS-CoV-2 RBD as the vaccine antigen. After confirming
431 that Circ-RBD vaccine induced a better overall response, we further evaluated its protective

432 efficacy, longevity of the immune response and compatibility for production of bivalent
433 vaccines using mouse model of the SARS-CoV-2 infection.
434 SAM-RNA was produced using the SFV replication machinery. SFV replicon was opted as
435 there are very few reports of SFV infection in human, with very mild symptoms and no
436 instances of mortality. SFV replicon has been used in earlier studies for heterologous protein
437 expression and a recently it has been used to produce a vaccine candidate against the Ebola
438 virus[34,35]. Also note that, multiple outbreaks of VEEV has been reported in North and South
439 American countries with cases of human death. Hence chances of anti-vector immunity is
440 higher in the case of VEEV[36].
441 The Anabaena permuted intron-exon sequence was used to produce the Circ-RNA and CVB3
442 IRES-mediated translation was used to produce the secretory signal and foldon fused-RBD
443 protein in the target cells. Circ-RNA vaccine production using the above vector has been
444 reported and well characterized[9]. Only the RBD region was used instead of the entire Spike
445 protein of the SARS-CoV-2 as it contains the majority of neutralizing epitopes, avoids induction
446 of antibody-dependent enhancement (ADE) and permits insertion of multiple elements due to
447 its smaller size. The trimeric structure of RBD was maintained using the foldon-motif to
448 improve its immunogenicity and virus neutralization potential, as reported earlier[37].
449 In order to compare the SAM-RBD vaccine with the Circ-RBD vaccine, it was important that
450 both vaccine antigens were expressed at comparable levels and did not induce the host innate
451 immune response. Western blot analysis using anti-RBD antibody and RT-qPCR analysis of
452 the ISGs confirmed that both vaccine candidates expressed similar levels of the vaccine
453 antigen and evaded the host innate immune pathway RNA sensors, respectively.
454 Although both SAM-RBD and Circ-RBD induced a similar humoral response, $CD4^+$ and $CD8^+$
455 memory T cell response was significantly increased in the Circ-RBD immunized mice. There
456 was a trend of increased production of IFNγ and TNFα in CD4+ and CD8+ memory T cells in
457 SAM-RBD immunized mice, however, it was not statistically significant, indicating that Circ-
458 RBD vaccine induced a more potent cell-mediated immune response. SFV replicon system
459 has been used to develop a dual antigen vaccine candidate against the Ebola virus by co-
460 expressing the viral glycoprotein and nucleoprotein where it was observed that high
461 intradermal dose of the Ebola virus glycoprotein induced IFNγ in CD4+ T cells and high
462 intradermal dose of nucleoprotein induced very low level of IFNγ in CD8+ T cells[35]. In the case
463 of VEEV-replicon based SARS-CoV-2-RBD and nucleocapsid (N)- expressing dual antigen
464 vaccine immunized outbred mice, IFNγ level was moderately increased in the CD4+ and CD8+
465 T cells stimulated with either the S- or N-peptide pool[38]. Other studies on evaluation of a SAM
466 vaccine candidate in mice based on the SARS-CoV-2-RBD or the Spike protein expressed
467 from an alpha virus (VEEV/ VEEV+Sindbis) replicon reported a significant T- cell response in

468 splenocytes of the immunized mice, upon stimulation with the S-peptide pool[39-42]. However,
469 SAM-Spike immunized pigtail macaques did not induce high level of IFNγ production in CD4+
470 and CD8+ T cells upon stimulation of splenocyte with S-peptide pool[40]. On the other hand, the
471 Circ-RBD vaccine of the SARS-CoV-2 induced similar level of T cell response as that of the
472 corresponding linear mRNA vaccine and a higher neutralizing antibody response than that of
473 the linear mRNA[9]. Given that different assays were conducted in different laboratories to
474 measure the T cell response, it is possible that lower IFNγ and TNFα production in CD4+ and
475 CD8+ T cells (splenocytes stimulated with RBD peptide pool) may be attributed to the overall
476 lesser sensitivity of our assay protocol. However, the relative difference in the level of IFNγ
477 and TNFα between SAM-RBD and Circ-RBD immunized sample would remain constant as
478 the samples were processed in parallel. Therefore, Circ-RBD vaccine appears to be a better
479 alternative to a SAM-RBD vaccine. Whether a VEEV replicon-based SAM vaccine shows a
480 similar profile as the SFV replicon used in our study, remains to be tested. A recent study also
481 showed potent adjuvant function of the circular RNA, irrespective of the antigen sequence and
482 robust CD8+ T-cell response induced by a circular RNA vaccine encoding the nucleoprotein
483 of the influenza virus, further supporting practical utility of the circular RNA vaccine
484 technology[10].
485 Functional efficacy of the Circ-RBD vaccine was characterized by evaluating its
486 thermostability, durability of the neutralizing antibody response, ability to protect the mice upon
487 SARS-CoV-2 challenge and compatibility as a bivalent vaccine formulation. Circ-RBD
488 immunization induced peak anti-RBD IgG titer at 4 weeks, which protected the mice from
489 COVID-19 like disease pathology when SARS-CoV-2 infection was initiated in the upper
490 respiratory tract (mild disease) or lower respiratory tract (severe disease, often leading to
491 lethality). Nine month follow up study of the anti-RBD IgG titer and the virus neutralization titer
492 (NT_{50}) did not show any decline in both. Moreover, neutralizing antibody titer was similar in
493 both male and female mice. With regard to stability of the Circ-RBD vaccine in normal
494 refrigeration conditions, there was no change in the characteristic of the Circ-RBD-LNP
495 formulation after 4 weeks of storage, however neutralizing antibody titer was stable for up to
496 2 weeks of storage. Finally, we evaluated the functional efficacy of a bivalent Circ-RBD
497 vaccine. Failure of monovalent vaccines in preventing COVID-19 for a longer period is
498 ascribed to emergence of newer variants of the SARS-CoV-2 containing escape mutations in
499 the RBD region. Bivalent vaccines based on linear mRNA platform or nanoparticle platform
500 expressing the spike protein or RBD region of the spike protein of the SARS-CoV-2-Delta and
501 Omicron variants have shown cross-protection against SARS-CoV-2 variants[28-30]. On similar
502 line, our data on the bivalent Circ-RBD vaccine expressing the RBD of Delta and Omicron
503 variants demonstrate cross-protection against the Wuhan, Delta and Omicron variants.

504 In summary, the current study compared the immunogenicity and virus neutralization efficacy
505 of the SAM and Circ-RNA vaccine candidates encoding the SARS-CoV-2-RBD antigen, which
506 revealed similar humoral immune response and virus neutralization potential of both vaccines
507 and a superior cell-mediated immune response induced by the later. Our data also showed
508 reasonable stability of the Circ-RNA vaccine at four degrees centigrade, high durability of the
509 neutralizing antibody response induced by it and high virus neutralization efficacy of the
510 bivalent Circ-RNA vaccine, all of which support the use of Circ-RNA technology in vaccine
511 development. An earlier study showed the superiority of the SARS-CoV-2 Circ-RNA vaccine
512 over the corresponding linear mRNA vaccine. Data obtained from this study further paves the
513 way for use of the Circ-RNA technology for vaccine development.
514

515 **Materials and Methods:**

516 **Plasmids and reagents**

517 Plasmid encoding the noninfectious Semliki Forest virus replicon (pSFV3) was a gift from
518 Henrik Garoff (Addgene plasmid # 92072 ; http://n2t.net/addgene:92072 ;
519 RRID:Addgene_92072)[34]. 988 to 1578 nucleotides encoding the RBD region (330 to 526
520 amino acids) of spike protein of the SARS-CoV-2 Wuhan isolate (hCoV-19/USA-WA1/2020)
521 fused in-frame with the CD5 secretory sequence at the N-terminal and the Bacteriophage T4
522 fibritin trimerization motif sequence at the C-terminus was synthesized and inserted into the
523 pSFV3 vector at the BamH1 restriction site. The resulting plasmid was named pSFV3-RBD.
524 Transcription of SFV-RBD hybrid RNA in the pSFV3-RBD vector was under control of the SP6
525 promoter. A circular RNA expression cassette containing the sequence of the T7 promoter,
526 Anabaena Group 1 intron 3' sequence, CVB3 IRES sequence, CD5 secretory sequence, RBD
527 region (988 to 1578 nucleotides) of spike protein of the SARS-CoV-2 Wuhan isolate (hCoV-
528 19/USA-WA1/2020), bacteriophage T4 fibritin trimerization motif and anabaena group 1 intron
529 5' sequence was chemically synthesised in the given order and cloned into the pUC57 vector.
530 The resulting plasmid was named pUC57 cRNA-RBD^{Wuhan}. RBD corresponding to the SARS-
531 CoV-2-Delta (hCoV-19/USA/MD-HP05285/2021) and Omicron (hCov-19/USA/MD-
532 HP2087/2021) variants were cloned similarly and the resulting plasmids were named pUC57
533 cRNA-RBD^{Del} and pUC57 cRNA-RBD^{Omi}, respectively. The goat anti-Mouse IgG-HRP
534 (Catalog No. 1030-05) was from Southern Biotech (Alabama, USA). Megascript SP6
535 transcription kit (Catalog no. AM1330), MegaScript T7 transcription kit (Catalog no. AM1334)
536 lipofectamine 3000 (Catalog No. L3000075), anti-SARS-CoV-2 Spike S1 (Catalog no. PA5-
537 81795), goat anti-Rabbit IgG-HRP (Catalog No. 31460), Anti-mouse IgG (H+L) Alexa Flour
538 488 (Catalog no. A28175) and Ribogreen (Catalog no. R11490) were from Thermo Fisher
539 Scientific (Massachusetts, USA). Scriptcap Cap 1 capping system (Catalog no. sccs1710) was
540 from CellScript (Wisconsin, USA). RNAse R (Catalog no. ab286929) was from Abcam

541 (Cambridge, United Kingdom). RNeasy Kit was from Qiagen ((Catalog no. 74104, Hilden,
542 Germany). SM102 (Catalog no. 33474) was from Cayman Chemical company (Michigan,
543 USA). DSPC (Catalog no. 850365P), Cholesterol (Catalog no. 700000P), and DMG-PEG
544 2000 (catalog no. 880151P), was from Sigma (Missouri, USA). Amicon ultra centrifugal filter
545 (Catalog no. UFC703008) was from Merck Millipore (Darmstadt, Germany). anti-GAPDH
546 antibody (Catalog no. SC-25778) was from Santa Cruz Biotechnology (Texas, USA). TRI-
547 reagent (Catalog no. TR118) was from MRC (Massachusetts, USA). Firescript cDNA
548 synthesis kit (Catalog no. 06-15-00050) and HOT FIREPol SolisGreen qPCR Mix (Catalog
549 no.08-47-0000S) from Solis Biodyne (Estonia). Ad5-hACE (catalog no. VVC-McCray-7723)
550 was obtained from the Viral Vector Core (University of Iowa, Iowa, USA). Vetbond (catalog
551 no. 1469Sb) was from 3M (Minnesota, USA). Mouse monoclonal antibody isotyping reagent
552 (Cat no. ISO2) was from Sigma Aldrich (Missouri, USA). SARS-CoV-2 spike antibody (catalog
553 no. GTX632604) was from GeneTex (California, USA). SARS-CoV-2 RBD peptide pool
554 (Catalog no: PM-WCPV-S_RBD-1) was from JPT innovative peptide solution (Berlin,
555 Germany). GolgiStop (Catalog no. 554724) was from BD bioscience (New Jersey, USA). FC
556 (Catalog no.14-9161-73), IC fixation buffer (Catalog no. FB001), permeabilizing buffer
557 (Catalog no. 00-8333-56), anti-mouse CD3 (Catalog no.100204), anti-mouse CD4 (Catalog
558 no.100408), anti-mouse CD8 (Catalog no.100714), anti-mouse CD44 (Catalog no.103030),
559 anti-mouse IFNγ (Catalog no. 505810), TNFα (Catalog no. 506328), and IL-4 (Catalog no.
560 504126) are from Thermo Fisher Scientific (Massachusetts, USA).
561
562 ***In vitro* transcription, capping, circularization, RNase R treatment and purification**
563 pSFV3-RBD, pUC57 cRNA-RBD^{Wuhan}, pUC57 cRNA-RBD^{Del} and pUC57 cRNA-RBD^{Omi}
564 plasmids were linearized and purified DNA was used for the *in vitro* transcription using the
565 Megascript SP6 or T7 transcription kit, following the manufacturer's instruction. SAM-RNA was
566 capped using the Scriptcap Cap 1 capping system, following the manufacturer's instructions.
567 In the case of Circ-RNA, *in vitro* transcribed RNA was incubated at 55^0C for 15 min in the
568 circularization buffer (10mM $MgCl_2$, 50mM Tris-HCl, 100mM NaCl, 1mM DTT, pH 7.9; New
569 England Biolabs, USA) and 2μM rGTP to circularize the RNA, as described earlier[16].
570 Circularized RNA was incubated at 37^0C for 7 min with 0.1units RNase R/μg RNA, followed
571 by addition of 0.1 units RNase R/μg RNA and incubation for another 7 min. RNA was purified
572 using the RNeasy kit, following the manufacturer's protocol (Qiagen, Germany).
573
574 **Preparation and characterization of the RNA-LNP vaccine formulation,**
575 SM102, DSPC, Cholesterol and DMG-PEG 2000 were mixed at a molar ratio of 50:10:38.5:1.5
576 in absolute ethanol at 1/5 of the final LNP amount. An aqueous solution of RNA was prepared

577 by diluting it in 50mM acetate buffer (1.2mM sodium acetate, 4mM acetic acid, pH 4.0) at 4/5
578 of the final LNP volume. The two solutions were mixed using a microfluidics system (ElveFlow
579 Elvesys, France) at a flow rate ratio of 1:5. The resulting RNA-LNP complex was dialyzed with
580 phosphate buffered saline (137 mM NaCl, 2.7 mM KCl, 10 mM Na_2HPO_4, 1.8 mM KH_2PO_4,
581 pH 6.8) and concentrated using a 30kDa MWCO Amicon ultra centrifugal filter to a volume of
582 0.1μg/μl RNA concentration. Further, the RNA-LNP vaccine formulation was passed through
583 a 0.2μm filter and aliquoted into glass vials and stored at 4^0C. Size and polydispersity (PDI) of
584 the RNA-LNP vaccine formulation was evaluated by dynamic light scattering (ZetaSizer lab,
585 Malvern panalytical, United Kingdom). For transmission electron microscopy (TEM), RNA-
586 LNP vaccine formulation was diluted ten times in H_2O, followed by staining with 2% uranyl
587 acetate and image acquisition using JEM-1400 Flash TEM equipped with tungsten filament
588 and sCMOS camera (JEOL Ltd, Japan). RNA encapsulation into LNP was measured by
589 fluorescent-based RNA quantification system using Ribogreen, following manufacturer's
590 instruction. The encapsulated RNA was released from the LNP by treating the RNA-LNP
591 vaccine formulation with 2% Triton X-100, followed by measurement of RNA quantity by
592 Ribogreen assay and evaluation of RNA quality by agarose gel electrophoresis.
593
594 **Mammalian cell culture, transfection, western blot, RT-qPCR, SARS-CoV-2 propagation**
595 HEK293T cells were maintained in Dulbecco's modified Eagle medium (DMEM)
596 supplemented with 10% FBS (fetal bovine serum) and Penicillin, Streptomycin during
597 maintenance. Cells were seeded on 6 well plates ($8x10^5$ cell/well) and transfected with 6μg
598 of RNA-LNP complex. Only LNP was added in the mock. For western blot analysis under
599 reducing condition, samples (cells or culture medium) were incubated at 95^0C for 5 minutes
600 in Laemlli buffer (2% SDS, 13% glycerol, 2.5% β-mercaptoethanol, 0.005% bromo phenol
601 blue and 63 mM Tris HCl, pH 6.8). For non-reducing condition, β-merceptoethanol was
602 omitted from the Laemlli buffer. Total protein in the samples was quantified by Bicinchoninic
603 acid assay and equal amount of protein were resolved in SDS-PAGE, followed by transfer to
604 Polyvinylidene fluoride (PVDF) membrane. The membrane was blocked with 5% skimmed
605 milk, incubated with anti-Spike S1 or anti-GAPDH antibody at 1:5000 dilution. Anti-Rabbit
606 secondary antibodies (Santa Cruz Biotechnology) were used at 1:5000 dilution. Protein
607 bands were developed by enhanced chemiluminescence reagent, using a commercially
608 available kit (BioRad, USA) and visualized in a gel Documentation system (Chemidoc MP,
609 Bio Rad, USA).
610 For RT-qPCR analysis of genes involved in the antiviral response pathway, HEK293T cells
611 were transfected with 1μg of SAM-RBD or Circ-RBD RNA or Poly I:C was using lipofectamine
612 3000, following manufacturer's instruction (Thermo Fisher Scientific, Massachusetts, USA).

613 24 hours post-transfection, total RNA was isolated using the TRI-reagent (MRC,
614 Massachusetts, USA), followed by reverse transcription (RT) using the Firescript cDNA
615 synthesis kit (Solis Biodyne, Estonia). The relative transcript levels of different genes were
616 determined by SYBR green based RT-qPCR, as described earlier[43]. Values obtained for
617 GAPDH RNA was used as an internal control for normalization of the data. Primer sequences
618 are as follows: hGAPDH FP: 5' GAGTCAACGGATTTGGTCGT 3', hGAPDH RP: 5'
619 TTGATTTTGGAGGGATCTCG 3', hIFNβ FP: 5' ACGCCGCATTGACCATCTAT 3', hIFNβ RP:
620 5' TTGGCCTTCAGGTAATGCAGA 3', hRIG-I FP: 5' TGTGGGCAATGTCATCAAAA 3', hRIG-
621 I RP: 5' GAAGCACTTGCTACCTCTTGC 3', hOASL FP; 5' AGGGTACAGATGGGACATCG
622 3', hOASL RP: 5' AAGGGTTCACGATGAGGTTG 3', hPKR FP: 5'
623 TCTTCATGTATGTGACACTGC 3', hPKR RP: 5' CACACAGTCAAGGTCCTT 3', hOAS1 FP:
624 5' GCTCCTACCCTGTGTGTGTGT 3', hOAS1 RP: 5' TGGTGAGAGTACTGAGGAAGA 3'.
625 For RT-qPCR analysis in the mouse lung tissue, total RNA was isolated from 10mg lung tissue
626 using TRI reagent, following manufacturer's instruction. cDNA synthesis and RT-qPCR was
627 done as mentioned above. HPRT RNA level was quantified for normalization of data. Primer
628 sequences are as follows: SCoV2 FP: 5' TGGACCCCAAAATCAGCGAA 3', SCoV2 RP: 5'
629 TCGTCTGGTAGCTCTTCGGT 3', mHPRT FP: 5' GTTGGATACAGGCCAGACTTTGTTG 3',
630 mHPRT RP: 5' GATTCAACTTGCGCTCATCTTAGGC 3', mIL-6 FP: 5'
631 GAGGATACCACTCCCAACAGACC 3', mIL-6 RP: 5' AAGTGCATCATCGTTGTTCATACA 3',
632 mIL-1β FP: 5' GCCCATCCTCTGTGACTCAT 3', mIL-1β RP: 5'
633 AGGCCACAGGTATTTTGTCG 3', mTNFα FP: 5' CATCTTCTCAAAATTCGAGTGACAA 3',
634 mTNFα RP: 5' TGGGAGTAGACAAGGTACAACCC 3', mIFNγ FP: 5'
635 AACGCTACACACTGCATCTTGG 3', mIFNγ RP: 5' GACTTCAAAGAGTCTGAGG 3'.
636 SARS-CoV-2 Wuhan isolate (NR-52281, SARS-related coronavirus-2 isolate ISA-WA1/2020)
637 and Omicron Variants (B.1.1.529, NR56461, SARS-related coronavirus-2 isolate hCoV-
638 19/USA/MD-HP20874/2021) were obtained from BEI Resources, amplified in Vero E6 cells in
639 the BSL3 facility of THSTI, India, titrated and stored frozen in aliquots. SARS-CoV-2-Delta
640 (SARS-CoV-2/human/IND/THSTI_287/2021) was isolated from clinical sample at THSTI and
641 has been reported (GenBank: MZ356566.1). SARS-CoV-2 infection was done as described[43].
642

643 **Mice handling, immunization, SARS-CoV-2 challenge study**

644 Mice were housed in individually ventilated cages at the experimental animal facility of THSTI.
645 For SARS-CoV-2 infection experiments, animals were housed in the animal biosafety level-3
646 (ABSL-3) laboratory of THSTI. Institutional animal ethics committee and institutional biosafety
647 committee approval was obtained for the experiments. Male and Female Balb/c mice of 6 to
648 8 weeks old were intradermally injected on the back of the animal. In the case of intramuscular

649 injection, mice were injected in the hind leg muscle. All injections were in 100μl volume.
650 Placebo animal received 100μl PBS. Blood was collected at the indicated time points through
651 retro-orbital sinus using a sterile hematocrit capillary tube. Wherever indicated, mice were
652 euthanized by anesthetic overdose (Ketamine 300 mg/kg and xylazine 30 mg/kg) and blood,
653 spleen and lungs were collected. Serum was isolated from the blood by centrifugation at
654 10,000g for 10 min at 4°C. Lung tissue was cut into parts and used for RNA, protein or
655 histopathology analysis.
656 SARS-CoV-2 challenge experiments were conducted in inbred Balb/c mice. Six to eight-week-
657 old mice were immunized with 10μg of Circ-RBD twice at two-weeks interval. Blood was
658 collected through retro-orbital sinus and anti-RBD IgG was measured. Replication deficient
659 adenovirus expressing human ACE2 (Ad5CMV-hACE2, denoted as hACE2) was transduced
660 through intranasal or intratracheal route[32,33]. For Intranasal transduction, mice were lightly
661 anaesthetized with isoflurane and $2x10^8$ pfu of hACE2 was administered, as described[32].
662 Intratracheal transduction of hACE2 was performed as described[33]. Mice were anaesthetised
663 with ketamine xylazine injection (Ketamine 100 mg/kg and xylazine 10 mg/kg), hair was
664 shaved from the neck region and a 5mm incision was made in the skin to expose the trachea.
665 $2x10^8$ pfu of hACE2 was administered in the trachea using a 24-gauge I.V. cannula. The
666 wound opening was glued with tissue adhesive (Vetbond, 3M Corp, USA). Animals did not
667 show any sign of illness or inflammation at the site of glue. Mice were infected with 10^5 pfu
668 SARS-CoV-2 intranasally after 5 days of hACE2 administration. Weight of the animals were
669 measured before infection and every day after the infection. In the intranasal transduction
670 model, mice were sacrificed 5 days post-SARS-CoV-2 infection and lung and BAL fluid were
671 harvested. In the case of intratracheal transduction model, weight was measured every day
672 after infection and survival was checked till 21 days of post-infection. When an animal showed
673 critical illness symptoms after SARS-CoV-2 infection, it was euthanized and samples were
674 collected. An animal from the immunized group was euthanized for comparison when mice
675 from the placebo group were euthanized.
676
677 **ELISA, Flow cytometry, quantification of viral load, virus Neutralization assay,**
678 The Enzyme-Linked Immunosorbent Assay (ELISA) was performed as described, with below
679 mentioned modifications[44]. The receptor-binding domains (RBDs) of the three SARS-CoV-2
680 variants-Wuhan, Delta, and Omicron, were expressed in-house in the Expi293 cells (Thermo
681 Fisher Scientific, Massachusetts, USA) and used in the ELISA. The assay samples (mice sera)
682 were diluted in a 3-fold series from 1:500 to 1:1,093,500. Horse radish peroxidase (HRP)-
683 labelled Goat anti-Mouse IgG (H+L) (Jackson ImmunoResearch, USA) was used at a dilution
684 of 1:5000. The endpoint anti-RBD IgG titer (denoted as anti-RBD IgG titer in the text and

685 figures) refers to the dilution factor at which the absorbance (obtained in the ELISA) of the
686 test samples exceeded three times that of the background (secondary Ab alone). Anti-RBD
687 IgM and IgG isotype (IgG1, IgG2a and IgG2b) ELISA was performed using a commercially
688 available kit, following the manufacturer protocol (Sigma Aldrich) at a serum dilution of 1:500.
689 For FACS study, splenocytes were prepared as described and cultured in RPMI-10
690 supplemented with 10%fetal bovine serum and 1% penicillin-streptomycin antibiotic[45]. After 3
691 hours, RBD peptide pool (2 μg/ml each peptide) and GolgiStop (BD) was added to the culture
692 medium for 6 hours. Cells were blocked with FC at room temperature for 15 min, stained with
693 anti-CD3, anti-CD4, anti-CD8 and anti-CD44 antibodies followed by fixation and
694 permeabilization. Intracellular staining of IFNγ, TNFα and IL-4 was performed using respective
695 antibodies. Cells were sorted using the BD FACS-aria (BD Biosciences) and data was
696 analyzed using the FlowJo software (FlowJo LLC, Oregon, USA).
697 For quantification of SARS-CoV-2 level in the lungs, 5mg of lung tissue was homogenised in
698 1ml serum free DMEM and sterilized using 0.2μm filter. The homogenate was serially diluted
699 10-fold and added to $2x10^5$ VeroE6 cells/well in 12 well plate for 1 hour. For quantification of
700 viral load in the BAL, BAL fluid were collected twice in PBS (500μl each), followed by passing
701 through 0.2μm filter. Two-fold serially diluted solution was added to $2x10^5$ VeroE6 cells/well in
702 12 well plate for 1 hour. Infection medium was removed, 1% carboxymethyl cellulose (CMC)
703 was added and plates were incubated for 48 hours at 37^0C, with 5% CO_2 supplementation.
704 Cells were fixed in 3.7% formaldehyde for overnight, plaques stained with 0.05% crystal violet
705 and number of plaques in each well was counted.
706 50% virus neutralization efficiency (NT_{50}) of the sera from mice immunized with the SAM-
707 RBD^{Wuhan} and Circ-RBD^{Wuhan} vaccine formulations (shown in Figs. 2D, 3E, 3F, 3H, 3J, S1B
708 and S1D) were measured by the Plaque reduction neutralization test (PRNT), as
709 described[46]. Briefly, mouse sera were heated at 55^0C for 30 min, 2-fold serially diluted
710 starting from 1:10 in serum-free DMEM, mixed with an equal volume of virus [virus stock was
711 appropriately diluted so that each well produces approximately 50 plaque forming units (pfu)]
712 and incubated at 37^0C for 1 hour. $2x10^5$ VeroE6 cells/well in 12 well plates were incubated
713 with the serum-virus mix for 1 hour. Infection medium was removed and cells were overlaid
714 with 1% CMC in 2% FBS supplemented DMEM and incubated at 37^0C with 5%CO_2
715 supplementation for 48 hours. Cells were fixed in 3.7% formaldehyde for overnight and
716 stained with 0.2% crystal violet. The number of plaques were counted and the serum dilution
717 leading to 50% neutralization of the virus (NT_{50}) was calculated using the GraphPad Prism
718 9.0 (Massachusetts, USA). NT_{50} of the Wuhan, Delta and Omicron variants (shown in
719 Figures 6F-6H) were measured by the Focus reduction neutralization test (FRNT). Heat
720 inactivated serum sample were 2- fold serially diluted, starting from 1:20 and mixed with an

721 equal volume of the virus [virus stock was appropriately diluted so that each well produces
722 approximately 100 focus forming units (ffu)] and incubated at 37^0C for 1 hour. $2x10^4$ VeroE6
723 cells/well in 96 well plates were incubated with the serum-virus mix for 1 hour. Infection
724 medium was removed and cells were overlaid with 0.5% CMC in 2% FBS supplemented
725 DMEM and incubated at 37^0C with 5%CO_2 supplementation for 24 hours. Cells were fixed in
726 formaldehyde and permeabilized with 0.2% Triton X-100. Next, the cells were stained with
727 anti-Spike antibody, following manufacturer's protocol followed by staining with alexa fluor-
728 488-conjugated anti-mouse IgG antibody. The number of foci was counted using an
729 ELISPOT reader (iSPOT, AID GmBh, Strassberg, Germany) and the serum dilution leading
730 to 50% neutralization of the virus was calculated using GraphPad Prism 9.0.

731 **Histopathology**

732 Histopathology analysis of the lung tissue samples were performed by the histology service of
733 the experimental animal facility of THSTI, following established protocol. Briefly, lung
734 tissues were kept in 10% neutral buffered formalin solution immediately after collection. After
735 ensuring proper fixation, samples were subjected to processing and paraffin embedded blocks
736 were prepared. 4μm thick sections were cut using a semi-automatic microtome (Histocore
737 Multicut- Leica Biosystem, Germany) and mounted on glass slides. The sections were stained
738 with haematoxylin and eosin, following standard operating procedures of the facility. Slides
739 were analysed by a qualified histopathologist, following blind evaluation method. Semi-
740 quantitative scoring system was adopted to score the pathological conditions, 0 indicating
741 absence of a pathological condition while 5 indicating its highest severity. Pathological
742 conditions such as; bronchiolitis, vasculitis, interstitial pneumonia, alveolitis and haemorrhage
743 were analysed and scored. Images were visualized and captured using a Bright field upright
744 microscope (CX43RF- Olympus Life science Solutions, Japan) equipped with a colour camera
745 (DP28- Olympus Life science Solutions, Japan) and imaging software (cellSens Entry-
746 Olympus Life science Solutions, Japan) at 200X magnification. Haematoxylin$^+$ area as an
747 index of cellularity was quantified from four different fields of 200X resolution using the ImageJ
748 software, as described[47].

749 **Statistical analysis**

750 All cell line data are derived from 3 independent experiments and represented as mean±SD
751 of 3 independent experiments. For mouse study, 6 or more animals were used in each group,
752 as indicated in the figures. Average values are shown in the bar and individual values are
753 shown as dots in each bar in the graphs. Two-tailed unpaired t-test (Mann-Whitney) and One-
754 way ANOVA (Kruskal-Wallis test) followed by Dunn's multiple comparisons was used for

comparison between groups, as indicated in the figures. Logistic regression was used to determine the NT_{50} titre of the mice sera. All statistical analysis was performed using the GraphPad Prism 9. A *p*-value <0.05 with 95% confidence interval was considered statistically significant.

Acknowledgement

This study was partly supported by a BIRAC (Biotechnology Industry Research Assistance Council, Department of Biotechnology, Government of India) grant to MS (BT/COVID0081/01/20) and THSTI core grant to MS. ONS and UB are supported by senior research fellowships from the Council of scientific and industrial research and the department of Biotechnology, Government of India, respectively. We are thankful to the experimental animal facility and biosafety level three (BSL3) facility of THSTI for helping with the experiments. The following reagent was deposited by the Centre for Disease Control and Prevention (USA) and obtained through BEI Resources, NIAID, NIH (USA): SARS-Related Coronavirus 2, isolate hCoV-19/USA-WA1/2020, NR-52281 and SARS-Related Coronavirus 2, isolate hCoV-19/USA/MD-HP20874/2021 (Lineage B.1.1.529; Omicron Variant), NR-56461, contributed by Andrew S. Pekosz. We are thankful to Henrik Garoff for the pSFV3 plasmid.

Author contribution

Conceptualization: MS; Investigation: ONS, UB, GJ, TRA, KC, SN, PS, SC, FM; Data analysis: ONS, GJ, TRA, BNP, SM, GB, CTRK, PG, MS; Resources: TS, SM, DN, GB, CTRK, PG, MS; manuscript writing: ONS, MS, GB, SM, CTRK. All authors have reviewed, edited and agreed to the final version of the manuscript.

Declaration of interest

The authors have no conflict of interest to declare.

Keywords: SARS-CoV-2, mRNA vaccine, self-amplifying mRNA, Circular mRNA, COVID-19, SARS-CoV-2 vaccine.

Reference

1. Thomas, S.J., Moreira Jr, E.D., Kitchin, N., Absalon, J., Gurtman, A., Lockhart, S., Perez, J.L., Pérez Marc, G., Polack, F.P., Zerbini, C., Bailey, R., et al. (2021). Safety

and efficacy of the BNT162b2 mRNA Covid-19 vaccine through 6 months. N. Engl. J. Med. 385, 1761-1773.

2. Baden, L.R., El Sahly, H.M., Essink, B., Kotloff, K., Frey, S., Novak, R., Diemert, D., Spector, S.A., Rouphael, N., Creech, C.B., et al. (2021). Efficacy and safety of the mRNA-1273 SARS-CoV-2 vaccine. N. Engl. J. Med. 384, 403-416.

3. Arevalo, C.P., Bolton, M.J., Le Sage, V., Ye, N., Furey, C., Muramatsu, H., Alameh, M.G., Pardi, N., Drapeau, E.M., Parkhouse, K., et al. (2022). A multivalent nucleoside-modified mRNA vaccine against all known influenza virus subtypes. Science 378, 899-904.

4. Krienke, C., Kolb, L., Diken, E., Streuber, M., Kirchhoff, S., Bukur, T., Akilli-Öztürk, Ö., Kranz, L.M., Berger, H., Petschenka, J., et al.(2021). A noninflammatory mRNA vaccine for treatment of experimental autoimmune encephalomyelitis. Science 371, 145-153.

5. Heine, A., Juranek, S., Brossart, P. (2021).Clinical and immunological effects of mRNA vaccines in malignant diseases. Mol. Cancer 20, 52.

6. Parhiz, H., Atochina-Vasserman, E.N., Weissman, D. (2024). mRNA-based therapeutics: looking beyond COVID-19 vaccines. The Lancet 403, 1192-1204.

7. Chaudhary, N., Weissman, D., Whitehead, K.A. (2021). mRNA vaccines for infectious diseases: principles, delivery and clinical translation. Nat. Rev. Drug Discov. 20, 817-838.

8. Saraf, A., Gurjar, R., Kaviraj, S., Kulkarni, A., Kumar, D., Kulkarni, R., Virkar, R., Krishnan, J., Yadav, A., Baranwal, E., et al. (2024). An Omicron-specific, self-amplifying mRNA booster vaccine for COVID-19: a phase 2/3 randomized trial. Nat. Med. 30, 1363-1372.

9. Qu, L., Yi, Z., Shen, Y., Lin, L., Chen, F., Xu, Y., Wu, Z., Tang, H., Zhang, X., Tian, F., et al. (2022). Circular RNA vaccines against SARS-CoV-2 and emerging variants. Cell 185, 1728-1744 e1716.

10. Amaya, L., Grigoryan, L., Li, Z., Lee, A., Wender, P.A., Pulendran, B., Chang, H.Y. (2023). Circular RNA vaccine induces potent T cell responses. Proc. Natl. Acad. Sci. USA 120, e2302191120.

11. Seephetdee, C., Bhukhai, K., Buasri, N., Leelukkanaveera, P., Lerdwattanasombat, P., Manopwisedjaroen, S., Phueakphud, N., Kuhaudomlarp, S., Olmedillas, E., Saphire, E.O., et al.(2022). A circular mRNA vaccine prototype producing VFLIP-X spike confers a broad neutralization of SARS-CoV-2 variants by mouse sera. Antiviral Res. 204, 105370.

12. Zhou, J., Ye, T., Yang, Y., Li, E., Zhang, K., Wang, Y., Chen, S., Hu, J., Zhang, K., Liu, F., et al. (2024). Circular RNA vaccines against monkeypox virus provide potent protection against vaccinia virus infection in mice. Mol. Ther. 32, 1779–1789.

13. Karikó, K., Muramatsu, H., Welsh, F.A., Ludwig, J., Kato, H., Akira, S., Weissman, D., (2008). Incorporation of pseudouridine into mRNA yields superior nonimmunogenic vector with increased translational capacity and biological stability. Mol. Ther. 16, 1833-1840.

14. Wang, X., Lu, Z., Gomez, A., Hon, G.C., Yue, Y., Han, D., Fu, Y., Parisien, M., Dai, Q., Jia, G., et al. (2014). N6-methyladenosine-dependent regulation of messenger RNA stability. Nature 505, 117-120.

15. Bloom, K., van den Berg, F., Arbuthnot, P. (2021). Self-amplifying RNA vaccines for infectious diseases. Gene therapy 28, 117-129.

16. Schmidt, C., Schnierle, B.S. (2023). Self-Amplifying RNA Vaccine Candidates: Alternative Platforms for mRNA Vaccine Development. Pathogens 12.

17. Pollock, K.M., Cheeseman, H.M., Szubert, A.J., Libri, V., Boffito, M., Owen, D., Bern, H., McFarlane, L.R., O'Hara, J., Lemm, N.M., et al. (2022). Safety and immunogenicity of a self-amplifying RNA vaccine against COVID-19: COVAC1, a phase I, dose-ranging trial. EClinicalMedicine 44, 101262.

18. Oda, Y., Kumagai, Y., Kanai, M., Iwama, Y., Okura, I., Minamida, T., Yagi, Y., Kurosawa, T., Greener, B., Zhang, Y., et al. (2024) Immunogenicity and safety of a booster dose of a self-amplifying RNA COVID-19 vaccine (ARCT-154) versus BNT162b2 mRNA COVID-19 vaccine: a double-blind, multicentre, randomised, controlled, phase 3, non-inferiority trial. Lancet Infect. Dis. 24, 351-360.

19. Liu, C.X., Chen, L.L. (2022). Circular RNAs: Characterization, cellular roles, and applications. Cell 185, 2016-2034.

20. Breuer, J., Barth, P., Noe, Y., Shalamova, L., Goesmann, A., Weber, F. and Rossbach, O. (2022). What goes around comes around: Artificial circular RNAs bypass cellular antiviral responses. Mol. Ther. Nucleic Acids 28, 623-635.

21. Wesselhoeft, R.A., Kowalski, P.S., Parker-Hale, F.C., Huang, Y., Bisaria, N., Anderson, D.G. (2019). RNA circularization diminishes immunogenicity and can extend translation duration in vivo. Mol. cell 74, 508-520. e504.

22. Wesselhoeft, R.A., Kowalski, P.S., Anderson, D.G. (2018). Engineering circular RNA for potent and stable translation in eukaryotic cells. Nat. Commun. 9, 2629.

23. Carabelli, A.M., Peacock, T.P., Thorne, L.G., Harvey, W.T., Hughes, J., Peacock, S.J., Barclay, W.S., De Silva, T.I., Towers, G.J., et al. (2023). SARS-CoV-2 variant biology: immune escape, transmission and fitness. Nat. Rev. Microbio. 21, 162-177.

24. Tao, K., Tzou, P.L., Nouhin, J., Gupta, R.K., de Oliveira, T., Kosakovsky Pond, S.L., Fera, D., Shafer, R.W. (2021). The biological and clinical significance of emerging SARS-CoV-2 variants. Nat. Rev. Genet. 22, 757-773.

25. Planas, D., Saunders, N., Maes, P., Guivel-Benhassine, F., Planchais, C., Buchrieser, J., Bolland, W.H., Porrot, F., Staropoli, I., Lemoine, F., et al. (2022). Considerable escape of SARS-CoV-2 Omicron to antibody neutralization. Nature 602, 671-675.

26. Liu, L., Iketani, S., Guo, Y., Chan, J.F.W., Wang, M., Liu, L., Luo, Y., Chu, H., Huang, Y., Nair, M.S., et al. (2022). Striking antibody evasion manifested by the Omicron variant of SARS-CoV-2. Nature 602, 676-681.

27. Cameroni, E., Bowen, J.E., Rosen, L.E., Saliba, C., Zepeda, S.K., Culap, K., Pinto, D., VanBlargan, L.A., De Marco, A., di Iulio, J., et al. (2022) Broadly neutralizing antibodies overcome SARS-CoV-2 Omicron antigenic shift. Nature 602, 664-670.

28. Corleis, B., Hoffmann, D., Rauch, S., Fricke, C., Roth, N., Gergen, J., Kovacikova, K., Schlottau, K., Halwe, N.J., Ulrich, L., et al. (2023) Efficacy of an unmodified bivalent mRNA vaccine against SARS-CoV-2 variants in female small animal models. Nat. Commun. 14, 816.

29. Li, J., Liu, Q., Liu, J., Fang, Z., Luo, L., Li, S., Lei, Y., Li, Z., Jin, J., Xie, R., et al. (2022) Development of Bivalent mRNA Vaccines against SARS-CoV-2 Variants. Vaccines (Basel) 10.

30. Yuan, Y., Zhang, X., Chen, R., Li, Y., Wu, B., Li, R., Zou, F., Ma, X., Wang, X., Chen, Q., et al. (2022). A bivalent nanoparticle vaccine exhibits potent cross-protection against the variants of SARS-CoV-2. Cell Rep. 38, 110256.

31. Piccoli, L., Park, Y.J., Tortorici, M.A., Czudnochowski, N., Walls, A.C., Beltramello, M., Silacci-Fregni, C., Pinto, D., Rosen, L.E., Bowen, J.E., et al. (2020). Mapping Neutralizing and Immunodominant Sites on the SARS-CoV-2 Spike Receptor-Binding Domain by Structure-Guided High-Resolution Serology. Cell 183, 1024-1042.

32. Hassan, A.O., Case, J.B., Winkler, E.S., Thackray, L.B., Kafai, N.M., Bailey, A.L., McCune, B.T., Fox, J.M., Chen, R.E., Alsoussi, W.B., et al. (2020). A SARS-CoV-2 Infection Model in Mice Demonstrates Protection by Neutralizing Antibodies. Cell 182, 744-753.

33. Gu, T., Zhao, S., Jin, G., Song, M., Zhi, Y., Zhao, R., Ma, F., Zheng, Y., Wang, K., Liu, H., et al. (2020). Cytokine Signature Induced by SARS-CoV-2 Spike Protein in a Mouse Model. Front. Immunol. 11, 621441.

34. Liljeström, P., Garoff, H. (1991). A new generation of animal cell expression vectors based on the Semliki Forest virus replicon. Nat. Biotech. 9, 1356-1361.

35. Krähling, V., Erbar, S., Kupke, A., Nogueira, S.S., Walzer, K.C., Berger, H., Dietzel, E., Halwe, S., Rohde, C., Sauerhering L., et al. (2023). Self-amplifying RNA vaccine protects mice against lethal Ebola virus infection. Mol. Ther. 31, 374-386.

36. Weaver, S.C., Salas, R., Rico-Hesse, R., Ludwig, G.V., Oberste, M.S., Boshell, J., Tesh, R.B. (1996). Re-emergence of epidemic Venezuelan equine encephalomyelitis in South America. Lancet 348, 436-440.

37. Routhu, N.K., Cheedarla, N., Bollimpelli, V.S., Gangadhara, S., Edara, V.V., Lai, L., Sahoo, A., Shiferaw, A., Styles, T.M., Floyd, K., et al. (2021). SARS-CoV-2 RBD trimer protein adjuvanted with Alum-3M-052 protects from SARS-CoV-2 infection and immune pathology in the lung. Nat. Commun. 12, 3587.

38. McCafferty, S., Haque, A.A., Vandierendonck, A., Weidensee, B., Plovyt, M., Stuchlíková, M., François, N., Valembois, S., Heyndrickx, L., Michiels, J., et al. (2022). A dual-antigen self-amplifying RNA SARS-CoV-2 vaccine induces potent humoral and cellular immune responses and protects against SARS-CoV-2 variants through T cell-mediated immunity. Mol. Ther. 30, 2968-2983.

39. McKay, P.F., Hu, K., Blakney, A.K., Samnuan, K., Brown, J.C., Penn, R., Zhou, J., Bouton, C.R., Rogers, P., Polra, K., et al. (2020). Self-amplifying RNA SARS-CoV-2 lipid nanoparticle vaccine candidate induces high neutralizing antibody titers in mice. Nat. Commun. 11, 3523.

40. Erasmus, J.H., Khandhar, A.P., O'Connor, M.A., Walls, A.C., Hemann, E.A., Murapa, P., Archer, J., Leventhal, S., Fuller, J.T., Lewis, T.B., et al. (2020). An Alphavirus-derived replicon RNA vaccine induces SARS-CoV-2 neutralizing antibody and T cell responses in mice and nonhuman primates. Sci. Transl. Med. 12, eabc9396.

41. De Alwis, R., Gan, E.S., Chen, S., Leong, Y.S., Tan, H.C., Zhang, S.L., Yau, C., Low, J.G., Kalimuddin, S., Matsuda, D., et al. (2021). A single dose of self-transcribing and replicating RNA-based SARS-CoV-2 vaccine produces protective adaptive immunity in mice. Mol. Ther. 29, 1970-1983.

42. Maruggi, G., Mallett, C.P., Westerbeck, J.W., Chen, T., Lofano, G., Friedrich, K., Qu, L., Sun, J.T., McAuliffe, J., Kanitkar, A., et al. (2022). A self-amplifying mRNA SARS-CoV-2 vaccine candidate induces safe and robust protective immunity in preclinical models. Mol. Ther. 30, 1897-1912.

43. Verma, R., Saha, S., Kumar, S., Mani, S., Maiti, T.K., Surjit, M. (2021). RNA-protein interaction analysis of SARS-CoV-2 5′ and 3′ untranslated regions reveals a role of lysosome-associated membrane protein-2a during viral infection. mSystems 6, 00643-00621.

44. Mehdi, F., Chattopadhyay, S., Thiruvengadam, R., Yadav, S., Kumar, M., Sinha, S.K., Goswami, S., Kshetrapal, P., Wadhwa, N., Chandramouli Natchu, U., et al. (2021). Development of a fast SARS-CoV-2 IgG ELISA, based on receptor-binding domain, and its comparative evaluation using temporally segregated samples from RT-PCR positive individuals. Front. Microbio. 11, 618097.

45. Agarwal, S., Kaur, S., Asuru, T.R., Joshi, G., Shrimali, N.M., Singh, A., Singh, O.N., Srivastva, P., Shrivastava, T., Vrati, S., et al. (2022). Dietary alpha-ketoglutarate inhibits SARS CoV-2 infection and rescues inflamed lungs to restore O(2) saturation by inhibiting pAkt. Clin. Transl. Med. 12, e1041.

46. Bewley, K.R., Coombes, N.S., Gagnon, L., McInroy, L., Baker, N., Shaik, I., St-Jean, J.R., St-Amant, N., Buttigieg, K.R., Humphries, H.E., et al. (2021). Quantification of SARS-CoV-2 neutralizing antibody by wild-type plaque reduction neutralization, microneutralization and pseudotyped virus neutralization assays. Nat. Protoc. 16, 3114-3140.

47. Chong, Z., Karl, C.E., Halfmann, P.J., Kawaoka, Y., Winkler, E.S., Keeler, S.P., Holtzman, M.J., Yu, J., Diamond, M.S. (2022). Nasally delivered interferon-lambda protects mice against infection by SARS-CoV-2 variants including Omicron. Cell Rep. 39, 110799.

Figure 1

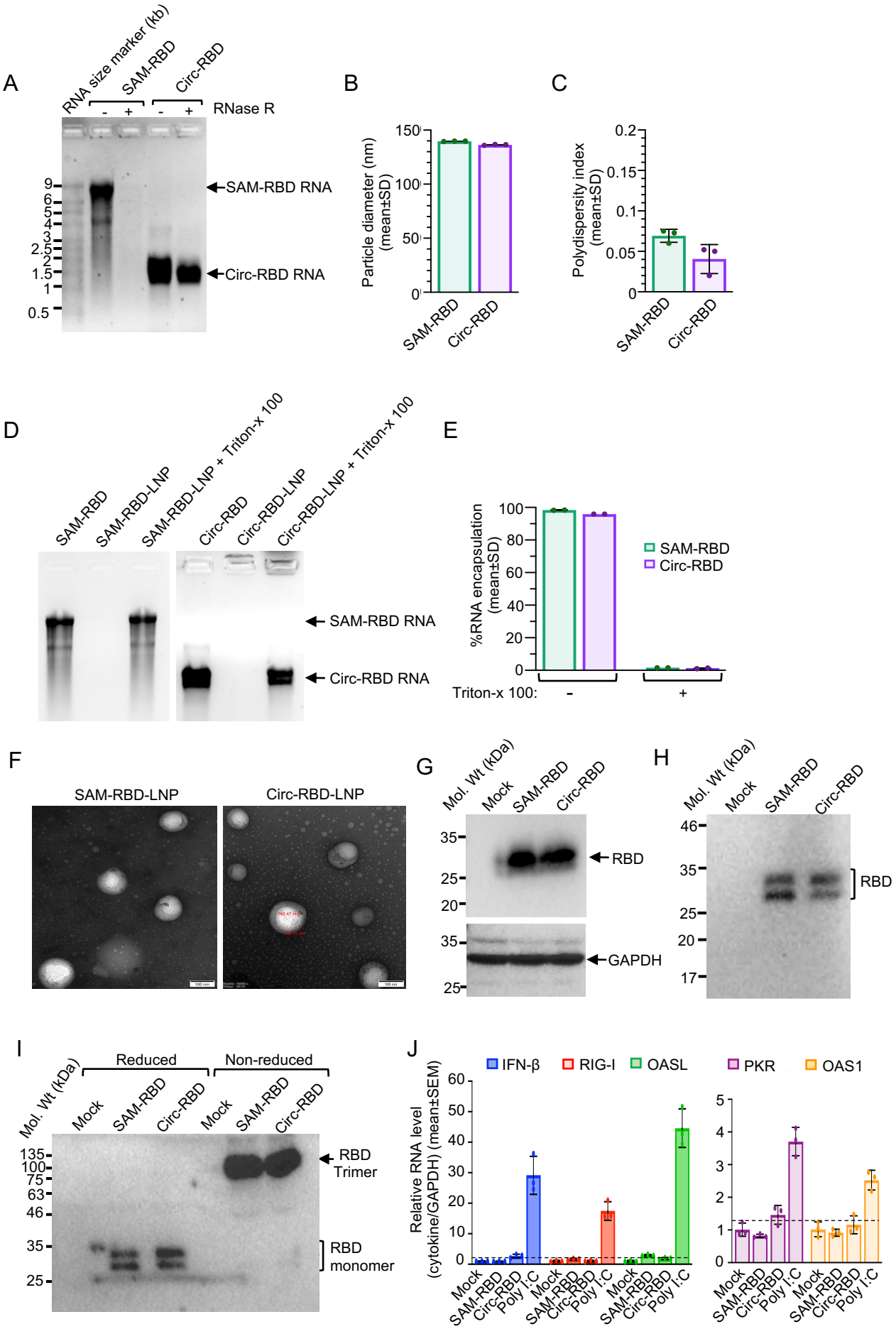
A
RNA size marker (kb)
SAM-RBD
Circ-RBD
RNase R
- + - +
9
6
5
4
3
2.5
2
1.5
1
0.5
SAM-RBD RNA
Circ-RBD RNA
B
Particle diameter (nm) (mean±SD)
150
100
50
0
SAM-RBD
Circ-RBD
C
Polydispersity index (mean±SD)
0.2
0.15
0.1
0.05
0
SAM-RBD
Circ-RBD
D
SAM-RBD
SAM-RBD-LNP
SAM-RBD-LNP + Triton-x 100
Circ-RBD
Circ-RBD-LNP
Circ-RBD-LNP + Triton-x 100
SAM-RBD RNA
Circ-RBD RNA
E
%RNA encapsulation (mean±SD)
100
80
60
40
20
0
SAM-RBD
Circ-RBD
Triton-x 100: - +
F
SAM-RBD-LNP
Circ-RBD-LNP
G
Mol. Wt (kDa)
Mock
SAM-RBD
Circ-RBD
35
25
20
RBD
35
25
GAPDH
H
Mol. Wt (kDa)
Mock
SAM-RBD
Circ-RBD
46
35
25
20
17
RBD
I
Mol. Wt (kDa)
Reduced
Non-reduced
Mock
SAM-RBD
Circ-RBD
Mock
SAM-RBD
Circ-RBD
135
100
75
63
46
35
25
RBD Trimer
RBD monomer
J
IFN-β
RIG-I
OASL
PKR
OAS1
Relative RNA level (cytokine/GAPDH) (mean±SEM)
60
50
40
30
20
10
0
5
4
3
2
1
0
Mock
SAM-RBD
Circ-RBD
Poly I:C

1007 **Figure Legends**

1008 **Figure 1. Production and characterization of the mRNA vaccine candidates.**

1009 (A) Agarose gel electrophoresis analysis of the *Invitro* transcribed and purified SAM-RBD and
1010 Circ-RBD RNA with (+) and without (-) treatment with RNase R.

1011 (B) Average particle size of SAM-RBD-RNA-LNP and Circ-RBD-RNA-LNP complex.

1012 (C) Average polydispersity Index of SAM-RBD-RNA-LNP and Circ-RBD-RNA-LNP complex.

1013 (D) Agarose gel electrophoresis analysis of the SAM-RBD and the Circ-RBD-RNA
1014 incorporation into the LNP. RNA-LNP formulations were treated with Triton-x-100, as
1015 indicated.

1016 (E) Average percent SAM-RBD and Circ-RBD RNA incorporation into the LNP. RNA-LNP
1017 formulations were treated with Triton-x-100, as indicated.

1018 (F) Scanning electron micrograph of SAM-RBD-LNP and Circ-RBD-LNP. Scale:100nm.

1019 (G) Western blot analysis of the RBD protein in HEK239T cells transfected with the SAM-
1020 RBD-LNP and Circ-RBD-LNP (upper panel). Mock: Lysate from HEK293T cells treated with
1021 LNP. Lower panel: Anti GAPDH western blot of aliquots of the cell lysate used in the upper
1022 panel.

1023 (H) Anti-RBD western blot of RBD protein in the cell culture medium of HEK239T cells
1024 mentioned in (G).

1025 (I) Anti-RBD western blot of aliquots of sample used in (H) under reducing and non-reducing
1026 conditions, as indicated.

1027 (J) RT-qPCR analysis of the indicated genes in total RNA isolated from HEK239T cells
1028 transfected with the SAM-RBD, Circ-RBD-RNA or poly I:C, as indicated. Mock: lipofectamine
1029 3000 transfected cells. PKR and OAS1 are shown in the right panel for clear representation.
1030 Dotted line indicates the background level. Data are mean±SD of three independent
1031 experiments. *P*-values were calculated by the non-parametric student's t-test, using the
1032 Mann-Whitney test.

1033

1034

1035

1036

1037

1038

1039

1040

1041

Figure 2

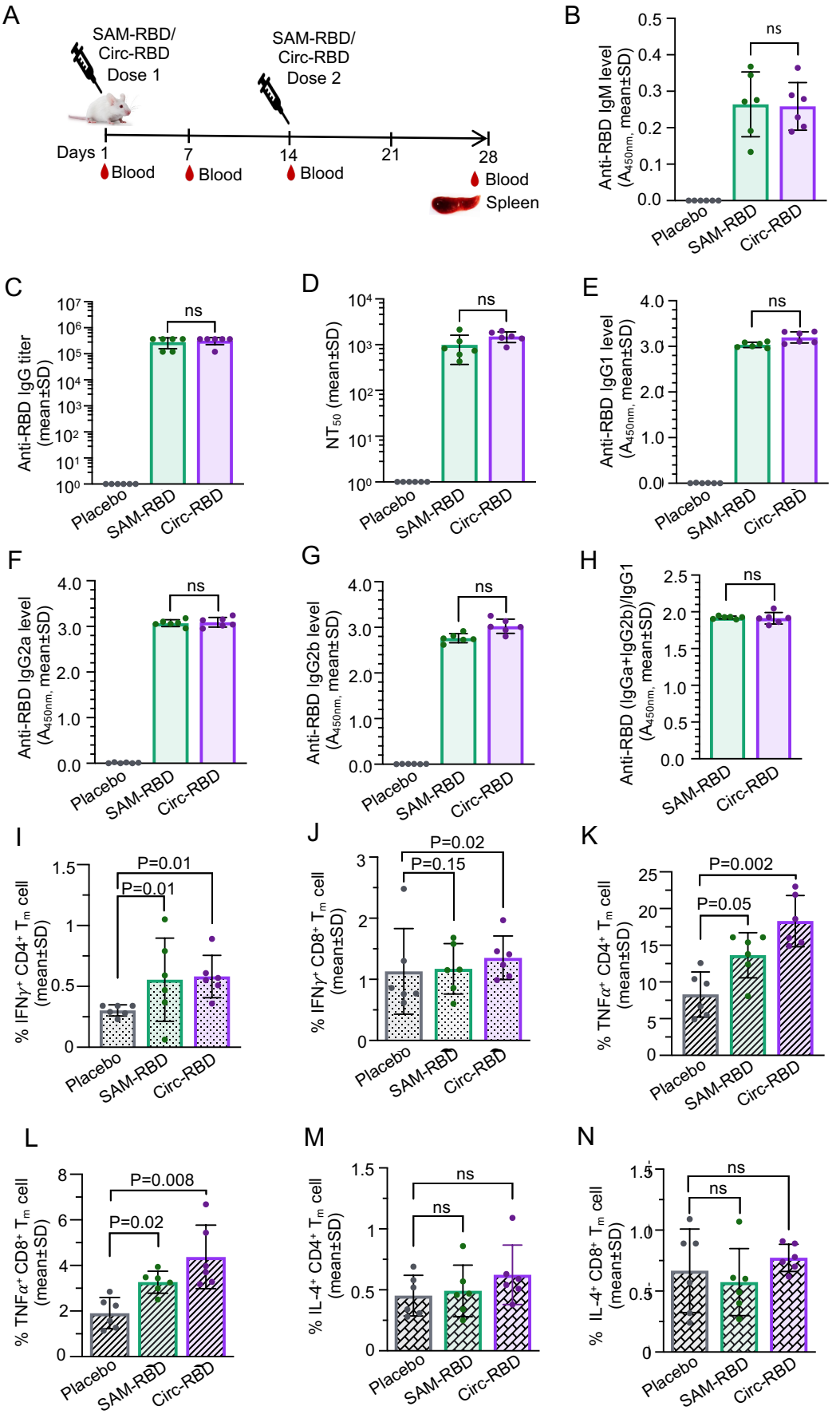
A
SAM-RBD/
Circ-RBD
Dose 1
SAM-RBD/
Circ-RBD
Dose 2
Days 1
7
14
21
28
Blood
Blood
Blood
Blood
Spleen
B
Anti-RBD IgM level
(A450nm, mean±SD)
ns
C
Anti-RBD IgG titer
(mean±SD)
ns
D
NT50 (mean±SD)
ns
E
Anti-RBD IgG1 level
(A450nm, mean±SD)
ns
F
Anti-RBD IgG2a level
(A450nm, mean±SD)
ns
G
Anti-RBD IgG2b level
(A450nm, mean±SD)
ns
H
Anti-RBD (IgGa+IgG2b)/IgG1
(A450nm, mean±SD)
ns
I
% IFNγ+ CD4+ Tm cell
(mean±SD)
P=0.01
P=0.01
J
% IFNγ+ CD8+ Tm cell
(mean±SD)
P=0.02
P=0.15
K
% TNFα+ CD4+ Tm cell
(mean±SD)
P=0.002
P=0.05
L
% TNFα+ CD8+ Tm cell
(mean±SD)
P=0.008
P=0.02
M
% IL-4+ CD4+ Tm cell
(mean±SD)
ns
ns
N
% IL-4+ CD8+ Tm cell
(mean±SD)
ns
ns
Placebo
SAM-RBD
Circ-RBD

1042 **Figure 2. Immunogenicity assessment of the SAM-RBD and Circ-RBD-RNA vaccine**
1043 **formulations.**
1044 (A) Schematic of the immunization study. Balb/c mice were intradermally injected with 10μg
1045 SAM-RBD or Circ-RBD-RNA-LNP on day 1 and 14. Blood was collected via retro-orbital route
1046 prior to the first immunization and subsequently on day 7 and day 28. Animals were euthanized
1047 on day 28, blood and spleen were collected.
1048 (B) Anti-RBD IgM level at 1 week post-immunization in the sera (1:500 dilution) of mice
1049 injected with the placebo (PBS), SAM-RBD and Circ-RBD-LNP, evaluated by ELISA.
1050 (C) Anti-RBD IgG titre at 4 weeks post-immunization in the sera of mice described in (B),
1051 evaluated by ELISA.
1052 (D) 50% virus neutralization titre (NT_{50}) at 4 weeks post-immunization in the sera of mice
1053 described in (B), evaluated by PRNT assay.
1054 (E) Anti-RBD IgG1 level (1:500 dilution) at 4 weeks post-immunization in the sera of mice
1055 described in (B), evaluated by ELISA.
1056 (F) Anti-RBD IgG2a level (1:500 dilution) at 4 weeks post-immunization in the sera of mice
1057 described in (B), evaluated by ELISA.
1058 (G) Anti-RBD IgG2b level (1:500 dilution) at 4 weeks post-immunization in the sera of mice
1059 described in (B), evaluated by ELISA.
1060 (H) Ratio of anti-RBD T_H1 antibody (IgG2a and IgG2b) to T_H2 (IgG1) antibody in the sera of
1061 mice injected with the SAM-RBD and Circ-RBD at 4 weeks, evaluated by ELISA.
1062 (I) Percentage of IFNγ and CD4 positive T-cells in the splenocytes, following stimulation with
1063 the SARS-CoV-2-Spike-RBD peptide pool, evaluated by FACS.
1064 (J) Percentage of IFNγ and CD8 positive T-cells in the splenocytes, following stimulation with
1065 the SARS-CoV-2-Spike-RBD peptide pool, evaluated by FACS.
1066 (K) Percentage of TNFα and CD4 positive T-cells in the splenocytes, following stimulation with
1067 the SARS-CoV-2-Spike-RBD peptide pool, evaluated by FACS.
1068 (L) Percentage of TNFα and CD8 positive T-cells in the splenocytes, following stimulation with
1069 the SARS-CoV-2-Spike-RBD peptide pool, evaluated by FACS.
1070 (M) Percentage of IL-4 and CD4 positive T-cells in the splenocytes, following stimulation with
1071 the SARS-CoV-2-Spike-RBD peptide pool, evaluated by FACS.
1072 (N) Percentage of IL-4 and CD8 positive T-cells in the splenocytes, following stimulation with
1073 the SARS-CoV-2- Spike-RBD peptide pool, evaluated by FACS.
1074 In all images, bars represent the average and dots represent the value obtained from each
1075 animal. Data are mean±SD, *p*-values were calculated by the non-parametric student's t-test,
1076 using the Mann-Whitney test (B-H) and the non-parametric one-way ANOVA, using the

Kruskal-wallis test (I-N). Values showing distinct difference from the majority in the group were not considered for calculating the *p*-value in the panels I-L.

Figure 3

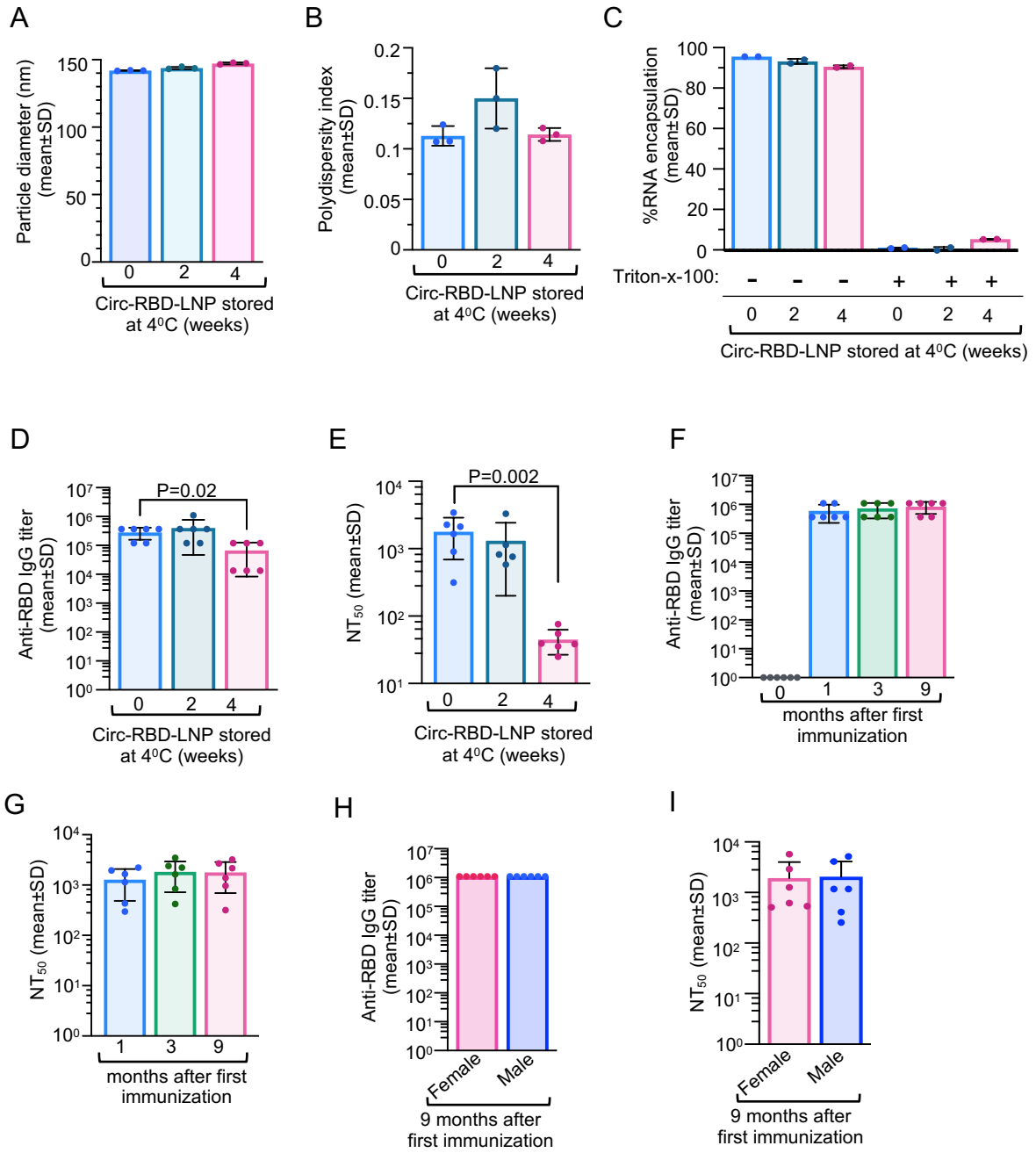
A
Particle diameter (nm) (mean±SD)
150
100
50
0
0
2
4
Circ-RBD-LNP stored at 4⁰C (weeks)
B
Polydispersity index (mean±SD)
0.2
0.15
0.1
0.05
0
0
2
4
Circ-RBD-LNP stored at 4⁰C (weeks)
C
%RNA encapsulation (mean±SD)
100
80
60
40
20
0
Triton-x-100:
-
-
-
+
+
+
0
2
4
0
2
4
Circ-RBD-LNP stored at 4⁰C (weeks)
D
Anti-RBD IgG titer (mean±SD)
P=0.02
0
2
4
Circ-RBD-LNP stored at 4⁰C (weeks)
E
NT50 (mean±SD)
P=0.002
0
2
4
Circ-RBD-LNP stored at 4⁰C (weeks)
F
Anti-RBD IgG titer (mean±SD)
0
1
3
9
months after first immunization
G
NT50 (mean±SD)
1
3
9
months after first immunization
H
Anti-RBD IgG titer (mean±SD)
Female
Male
9 months after first immunization
I
NT50 (mean±SD)
Female
Male
9 months after first immunization

1113 **Figure 3. Stability and durability of the immune response induced by the Circ-RBD-LNP**
1114 **vaccine formulation.**
1115 (A) Average size of the Circ-RBD-LNP stored at 4^0C for 0, 2 and 4 weeks, evaluated by
1116 dynamic light scattering.
1117 (B) Average polydispersity index of the Circ-RBD-LNP, stored as indicated in (A).
1118 (C) Percentage of RNA encapsulated into the LNP in the Circ-RBD-LNP formulation, stored
1119 as indicated in (A). Equal aliquots of the samples were treated with the Triton X-100.
1120 (D) Anti-RBD IgG titre in the sera of mice immunized for 4 weeks with the Circ-RBD-LNP,
1121 stored as indicated in (A).
1122 (E) 50% virus neutralization titre (NT_{50}) in aliquots of the sera used in (D), evaluated by PRNT
1123 assay.
1124 (F) Anti-RBD IgG titre at 0, 1, 3 and 9 months post-immunization in the sera of mice immunized
1125 with the Circ-RBD-LNP, evaluated by ELISA.
1126 (G) 50% virus neutralization titre (NT_{50}) in aliquots of the sera described in (G), evaluated by
1127 PRNT assay.
1128 (H) Anti-RBD IgG titre at 9 months post-immunization with the Circ-RBD-LNP, in male and
1129 female mice, evaluated by ELISA.
1130 (I) 50% virus neutralization titre (NT_{50}) in aliquots of the sera described in (I), evaluated by
1131 PRNT assay.
1132 Data are mean±SD of triplicate samples (A-C) and six mice/group (D-I), *p*-values were
1133 determined by the unpaired student's t-test, using the Mann-Whitney test.
1134
1135
1136
1137
1138
1139
1140
1141
1142
1143
1144
1145
1146
1147
1148

Figure 4

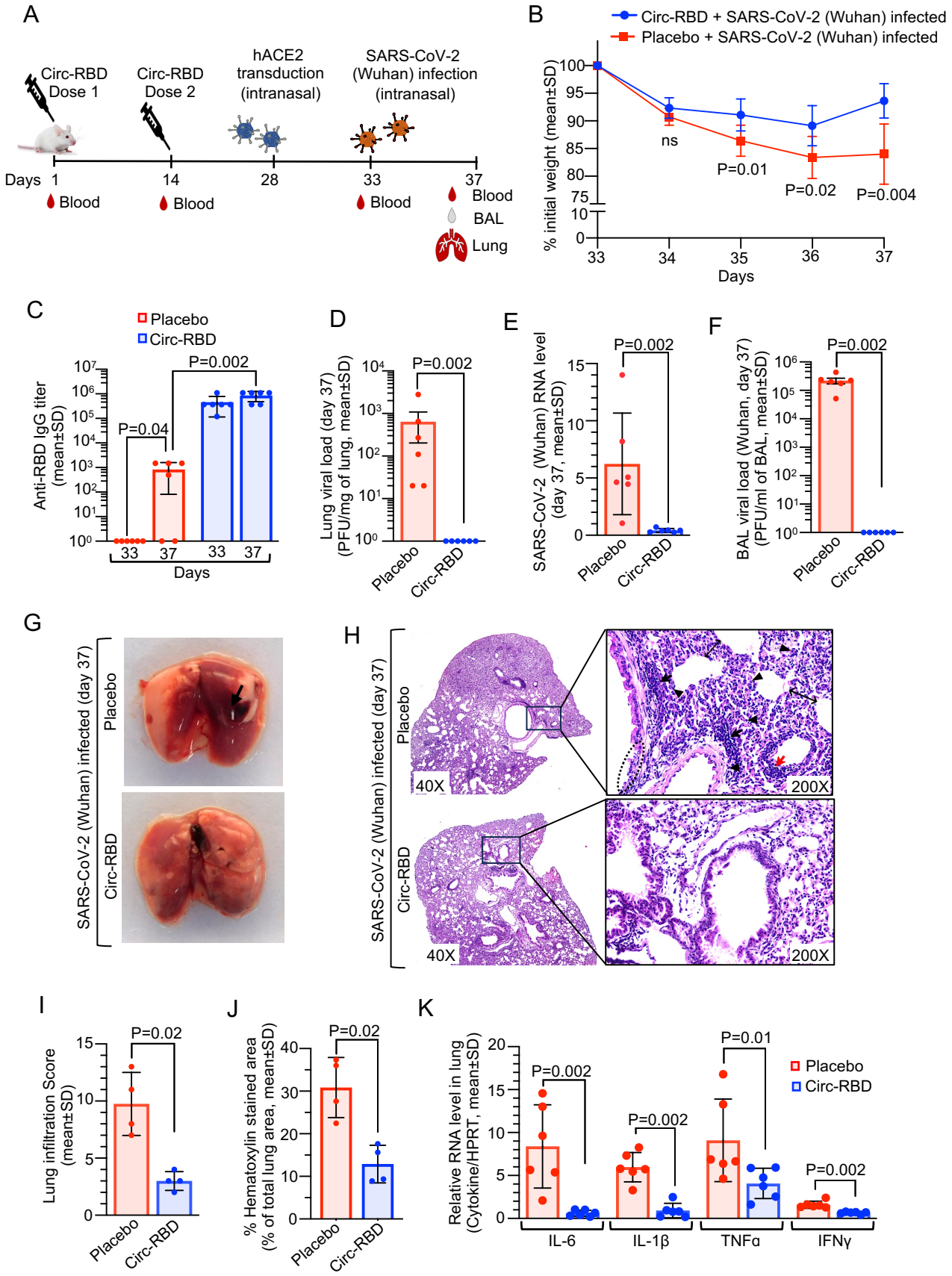
A
Circ-RBD Dose 1
Circ-RBD Dose 2
hACE2 transduction (intranasal)
SARS-CoV-2 (Wuhan) infection (intranasal)
Days 1 14 28 33 37
Blood
Blood
Blood
Blood
BAL
Lung
B
Circ-RBD + SARS-CoV-2 (Wuhan) infected
Placebo + SARS-CoV-2 (Wuhan) infected
% initial weight (mean±SD)
ns
P=0.01
P=0.02
P=0.004
Days
C
Placebo
Circ-RBD
Anti-RBD IgG titer (mean±SD)
P=0.04
P=0.002
Days
D
Lung viral load (day 37) (PFU/mg of lung, mean±SD)
P=0.002
Placebo
Circ-RBD
E
SARS-CoV-2 (Wuhan) RNA level (day 37, mean±SD)
P=0.002
Placebo
Circ-RBD
F
BAL viral load (Wuhan, day 37) (PFU/ml of BAL, mean±SD)
P=0.002
Placebo
Circ-RBD
G
SARS-CoV-2 (Wuhan) infected (day 37)
Placebo
Circ-RBD
H
SARS-CoV-2 (Wuhan) infected (day 37)
Placebo
Circ-RBD
40X
200X
40X
200X
I
Lung infiltration Score (mean±SD)
P=0.02
Placebo
Circ-RBD
J
% Hematoxylin stained area (% of total lung area, mean±SD)
P=0.02
Placebo
Circ-RBD
K
Relative RNA level in lung (Cytokine/HPRT, mean±SD)
Placebo
Circ-RBD
P=0.002
P=0.002
P=0.01
P=0.002
IL-6
IL-1β
TNFα
IFNγ

1149 **Figure 4. Immunization with the Circ-RBD protects mice from intranasal SARS-CoV-2**
1150 **challenge-induced disease symptoms.**
1151 (A) Schematic of the Circ-RBD-LNP immunization and the SARS-CoV-2 challenge study in
1152 mice. Blood was collected before immunization on day 1 and day 14. Mice were injected with
1153 the Circ-RBD-LNP or PBS (placebo group) on day 1 and day 14. Intranasal transduction of
1154 the hACE2 was done on day 28, followed by intranasal administration of the SARS-CoV-2
1155 (Wuhan) on day 33. Mouse weight was measured every day from day 33 to day 37. Mice were
1156 euthanized on day 37 and blood, lung tissue, bronchoalveolar lavage (BAL) were collected.
1157 (B) Effect of the SARS-CoV-2 (Wuhan) infection on mice weight. Weight of each mouse in the
1158 placebo and the Circ-RBD immunization group was measured (N=6) every day from day 33-
1159 37 and the average of percent weight change with respect to the weight on day 33 (considered
1160 100%) is plotted in the graph.
1161 (C) Anti-RBD IgG titre in sera of the placebo and the Circ-RBD immunized, SARS-CoV-2
1162 (Wuhan) infected mice, as indicated in (A). Sera collected on day 33 and 37 were evaluated
1163 by ELISA.
1164 (D) Measurement of viral load (SARS-CoV-2,Wuhan) in the lung tissue of the placebo and the
1165 Circ-RBD immunized mice. Samples were collected on day 37, as indicated in (A) and viral
1166 load was measured by plaque assay.
1167 (E) Measurement of viral RNA level in aliquots of the lung tissue described in (D), determined
1168 by RT-qPCR.
1169 (F) Measurement of viral load in the BAL of the placebo and the Circ-RBD immunized, SARS-
1170 CoV-2 (Wuhan) infected mice, collected on day 37 and evaluated by plaque assay.
1171 (G) Lung morphology of the placebo and the Circ-RBD immunized, SARS-CoV-2 (Wuhan)
1172 infected mice, collected on day 37.
1173 (H) Hematoxylin and eosin-stained image of lung tissue section prepared from the placebo
1174 and Circ-RBD immunized, SARS-CoV-2 (Wuhan) infected mice, collected on day 37. Images
1175 were acquired at 40X (left panel) and 200X (right panel) magnification. Black and red arrows
1176 indicate peribronchiolar and perialveolar infiltration, respectively, black arrow-head indicates
1177 neutrophils, double headed black arrow indicates alveolar septa thickening and dotted region
1178 indicates epithelial damage.
1179 (I) Lung infiltration score of the placebo and Circ-RBD immunized, SARS-CoV-2 (Wuhan)
1180 infected mice, evaluated by analysis of the hematoxylin and eosin-stained images of tissue
1181 sections prepared from the lungs collected on day 37.
1182 (J) Percentage of hematoxylin-stained area in the hematoxylin and eosin-stained images of
1183 lung tissue section of the placebo and Circ-RBD immunized, SARS-CoV-2 (Wuhan) infected
1184 mice, shown in (H).

(K) RT-qPCR analysis of the indicated cytokines in the total RNA isolated from lung tissue of the placebo and Circ-RBD immunized, SARS-CoV-2 (Wuhan) infected mice.
Data are shown as the mean±SD, *p*-values were determined by the unpaired student's t-test, using the Mann-Whitney test.

Figure 5

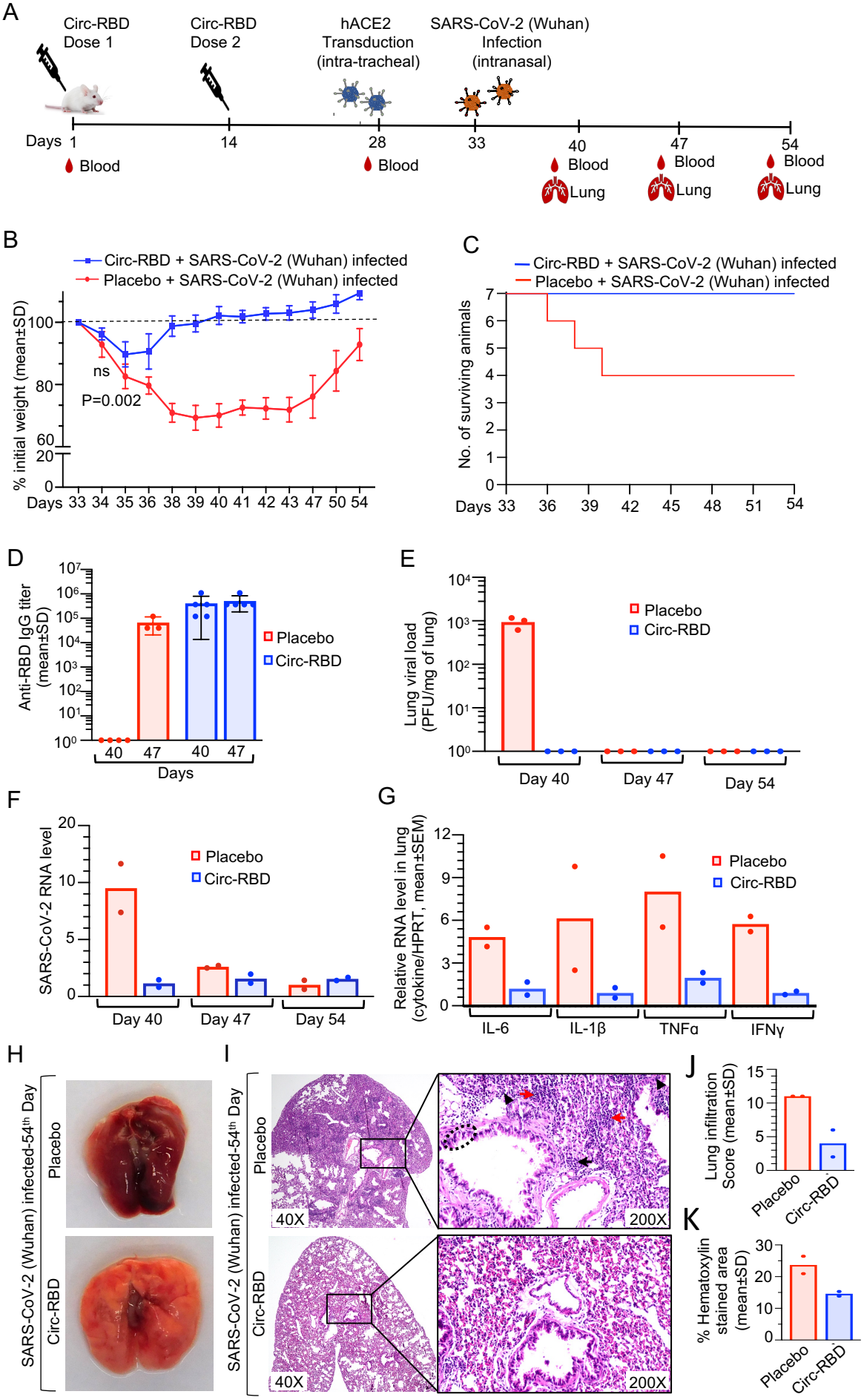
A
Circ-RBD Dose 1
Circ-RBD Dose 2
hACE2 Transduction (intra-tracheal)
SARS-CoV-2 (Wuhan) Infection (intranasal)
Days 1 14 28 33 40 47 54
Blood
Lung
B
Circ-RBD + SARS-CoV-2 (Wuhan) infected
Placebo + SARS-CoV-2 (Wuhan) infected
% initial weight (mean±SD)
ns
P=0.002
Days 33 34 35 36 38 39 40 41 42 43 47 50 54
C
No. of surviving animals
Days 33 36 39 42 45 48 51 54
D
Anti-RBD IgG titer (mean±SD)
Placebo
Circ-RBD
Days
E
Lung viral load (PFU/mg of lung)
Day 40
Day 47
Day 54
F
SARS-CoV-2 RNA level
G
Relative RNA level in lung (cytokine/HPRT, mean±SEM)
IL-6
IL-1β
TNFα
IFNγ
H
SARS-CoV-2 (Wuhan) infected-54th Day
I
40X
200X
J
Lung infiltration Score (mean±SD)
K
% Hematoxylin stained area (mean±SD)

1221 **Figure 5. Immunization with the Circ-RBD protects mice from the intratracheal SARS-**
1222 **CoV-2 challenge-induced disease symptoms.**
1223 (A) Schematic of the Circ-RBD-LNP immunization and the SARS-CoV-2 challenge study in
1224 mice. Blood was collected before immunization on day 1 and day 14. Mice were injected with
1225 the Circ-RBD-LNP or PBS (placebo group) on day 1 and day 14. Intra-tracheal transduction
1226 of the hACE2 was done on day 28, followed by intranasal infection with the SARS-CoV-2
1227 (Wuhan) on day 33. Mouse weight was measured every day from day 33-54. Mice were
1228 euthanized on day 40, 47 and 54 and blood and lung tissue were collected.
1229 (B) Effect of the SARS-CoV-2 (Wuhan) infection on mice weight. Weight of each mouse in the
1230 placebo and the Circ-RBD immunization group was measured (initial no. of mice in both
1231 groups = 7) on the indicated days between day 33 to day 54 and the average of percent weight
1232 change with respect to the weight on day 33 (considered 100%) is plotted in the graph. Few
1233 animals in the placebo group died during the experimental period, as indicated in (D). Average
1234 weight of the remaining animals is plotted.
1235 (C) Survival of mice in the placebo and the Circ-RBD immunized group was monitored every
1236 day from day 33 to day 54.
1237 (D) Anti-RBD IgG titre in the sera of the placebo and Circ-RBD immunized, SARS-CoV-2
1238 (Wuhan) infected mice as indicated in (A). Sera collected on day 40 and day 47 were evaluated
1239 by ELISA.
1240 (E) Measurement of viral load (SARS-CoV-2,Wuhan) in lung tissue of the placebo and Circ-
1241 RBD immunized, SARS-CoV-2 (Wuhan) infected mice, evaluated by plaque assay.
1242 (F) Measurement of the viral RNA level in aliquots of the lung tissue described in (E),
1243 determined by RT-qPCR.
1244 (G) RT-qPCR analysis of the indicated cytokines in the total RNA isolated from lung tissue of
1245 the placebo and Circ-RBD immunized, SARS-CoV-2 (Wuhan) infected mice, collected on day
1246 54.
1247 (H) Lung morphology of the placebo and Circ-RBD immunized, SARS-CoV-2 (Wuhan)
1248 infected mice, collected on day 54.
1249 (I) Representative hematoxylin and eosin-stained image of lung tissue section prepared from
1250 the placebo and Circ-RBD immunized, SARS-CoV-2 (Wuhan) infected mice, collected on day
1251 54. Images were acquired at 40X (left panel) and 200X magnification (right panel). Black and
1252 red arrow indicate peribronchiolar and perialveolar infiltration, respectively; black arrow-head
1253 indicate neutrophils, double headed black arrow indicates alveolar septa thickening and dotted
1254 region indicates epithelial damage.
1255 (J) Lung infiltration score of the placebo and Circ-RBD immunized, SARS-CoV-2 (Wuhan)
1256 infected mice, evaluated by analysis of the hematoxylin and eosin-stained images of tissue
1257 sections prepared from the lung tissue collected on day 54.

(K) Percentage of hematoxylin-stained area in the hematoxylin and eosin-stained images of lung tissue section of the placebo and Circ-RBD immunized, SARS-CoV-2 (Wuhan) infected mice, collected on day 54.

In (B) and (D), data are shown as the mean±SD and *p*-values were determined by the unpaired student's t-test, using the Mann-Whitney test.

Figure 6

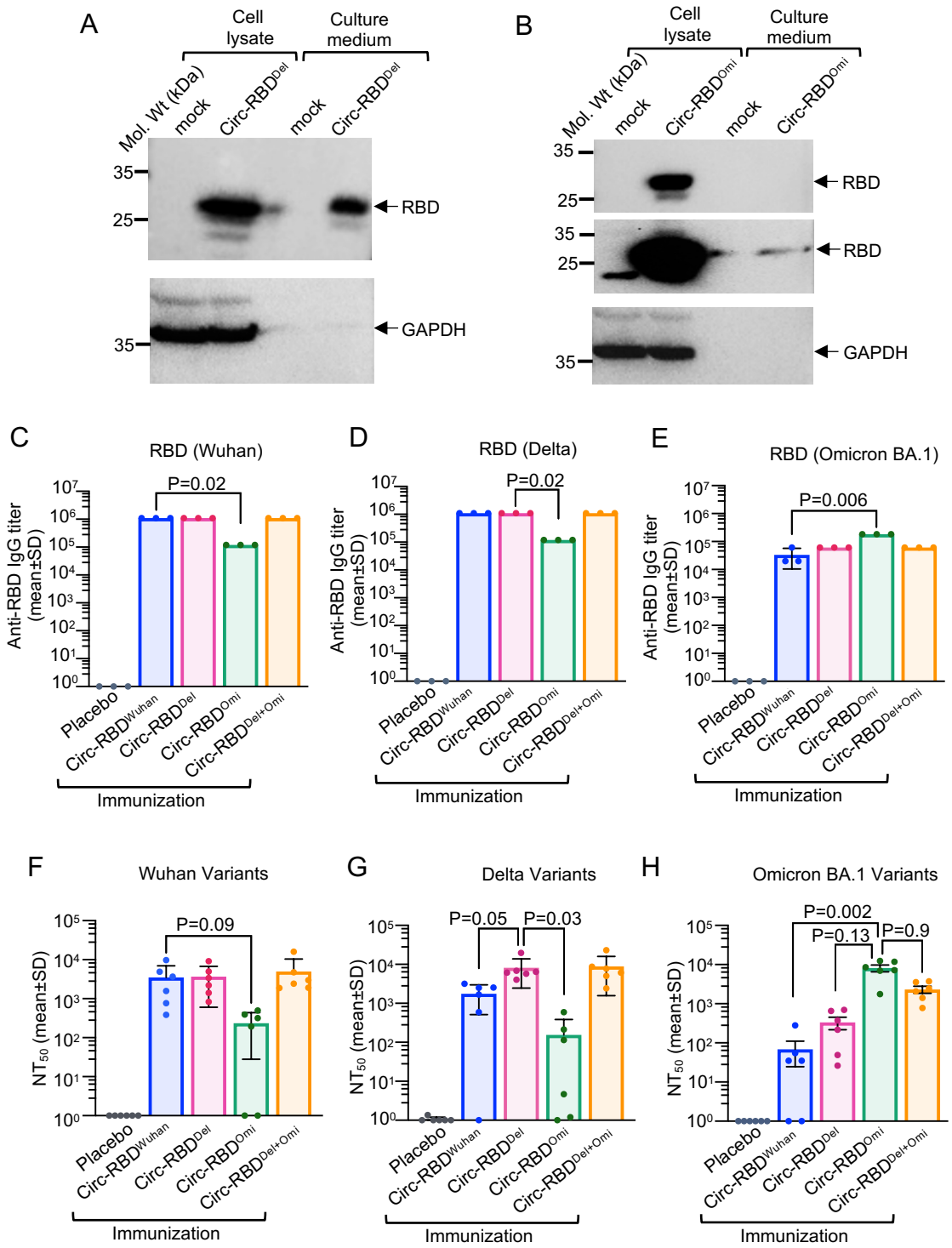
A
Cell lysate
Culture medium
Mol. Wt (kDa)
mock
Circ-RBD^{Del}
mock
Circ-RBD^{Del}
35
25
RBD
35
GAPDH
B
Cell lysate
Culture medium
Mol. Wt (kDa)
mock
Circ-RBD^{Omi}
mock
Circ-RBD^{Omi}
35
25
RBD
35
25
RBD
35
GAPDH
C
RBD (Wuhan)
P=0.02
Anti-RBD IgG titer (mean±SD)
Placebo
Circ-RBD^{Wuhan}
Circ-RBD^{Del}
Circ-RBD^{Omi}
Circ-RBD$^{Del+Omi}$
Immunization
D
RBD (Delta)
P=0.02
Anti-RBD IgG titer (mean±SD)
Immunization
E
RBD (Omicron BA.1)
P=0.006
Anti-RBD IgG titer (mean±SD)
Immunization
F
Wuhan Variants
P=0.09
NT_{50} (mean±SD)
Immunization
G
Delta Variants
P=0.05
P=0.03
NT_{50} (mean±SD)
Immunization
H
Omicron BA.1 Variants
P=0.002
P=0.13
P=0.9
NT_{50} (mean±SD)
Immunization

Figure 6. Assessment of immunogenicity and virus neutralization potential of the Circ-RBD^{Del} and Circ-RBD^{Omi} bivalent vaccine formulation.

(A) Western blot analysis of the RBD protein in the HEK239T cells transfected with the Circ-RBD^{Del}-LNP (upper panel). Mock: HEK293T cells treated with LNP. Lower panel: Anti GAPDH western blot of aliquots of the samples used in the upper panel.

(B) Western blot analysis of the RBD protein in the HEK239T cells transfected with the Circ-RBD^{Omi}-LNP (upper panel-lower exposure, middle panel-higher exposure of the same blot). Mock: HEK293T cells treated with LNP. Lower panel: anti GAPDH western blot of aliquots of the samples used in the upper panel.

(C) Anti-RBD^{Wuhan} IgG titre at 4 weeks post-immunization in the sera of mice injected with the placebo (PBS), Circ-RBD^{Wuhan}, Circ-RBD^{Del}, Circ-RBD^{Omi} and bivalent Circ-RBD^{Del}+Circ-RBD^{Omi} vaccine formulations, evaluated by ELISA.

(D) Anti-RBD^{Del} IgG titre at 4 weeks post-immunization in the sera of mice described in (C), evaluated by ELISA.

(E) Anti-RBD^{Omi} IgG titre at 4 weeks post-immunization in the sera of mice described in (C), evaluated by ELISA.

(F) 50% virus neutralization titre (NT_{50}) against the SARS-CoV-2 (Wuhan) at 4 weeks post-immunization in the sera of mice described in (C), evaluated by FRNT assay.

(G) 50% virus neutralization titre (NT_{50}) against the SARS-CoV-2 (Delta) at 4 weeks post-immunization in the sera of mice described in (C), evaluated by FRNT assay.

(H) 50% virus neutralization titre (NT_{50}) against the SARS-CoV-2 (Omicron BA.1) at 4 weeks post-immunization in the sera of mice described in (C), evaluated by FRNT assay.

In (C)-(E), data are shown as the mean±SD of pooled sera of 6 animals in each group, assayed in triplicate. In (F)-(H), data are shown as the mean±SD of 6 animals in each group, assayed individually. *p*-values were determined by the non-parametric one-way ANOVA, using the Kruskal-wallis test.

Figure S1

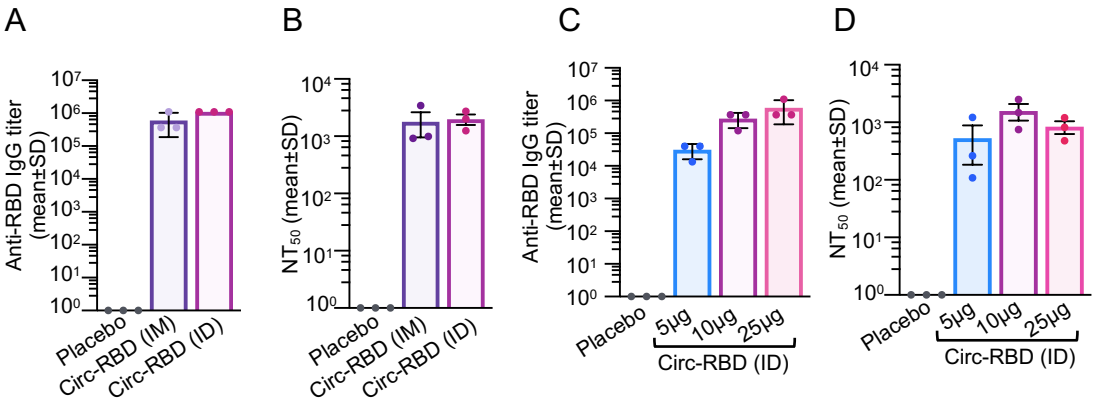
A
B
C
D
Anti-RBD IgG titer (mean±SD)
NT50 (mean±SD)
Placebo
Circ-RBD (IM)
Circ-RBD (ID)
5μg
10μg
25μg
Circ-RBD (ID)

1330 **Supplementary Figure legends**

1331 **Figure S1. Selection of immunization route and dose of RNA-LNP formulation that**
1332 **elicits significant immune response in mice.**

1333 (A) Anti-RBD IgG titre at 4 weeks post-immunization in the sera of mice injected with the
1334 placebo (PBS) and the Circ-RBD-LNP via intramuscular (IM) or intradermal (ID) route,
1335 evaluated by ELISA.

1336 (B) 50% virus neutralization titre (NT_{50}) at 4 weeks post-immunization in the sera of mice
1337 described in (B), evaluated by PRNT assay.

1338 (C) Anti-RBD IgG titre at 4 weeks post-immunization in the sera of mice intradermally injected
1339 with the placebo (PBS) or 5, 10, 25μg of Circ-RBD-LNP, evaluated by ELISA.

1340 (D) 50% virus neutralization titre (NT_{50}) at 4 weeks post-immunization in the sera of mice
1341 described in (C), evaluated by PRNT assay.

1342 Data are shown as the mean±SD of pooled sera from five animals, assayed in triplicate; *p*-
1343 values were determined by the unpaired student's t-test, using the Mann-Whitney test.

1344
1345
1346
1347
1348
1349
1350
1351
1352
1353
1354
1355
1356
1357
1358
1359
1360
1361
1362
1363

Figure S2

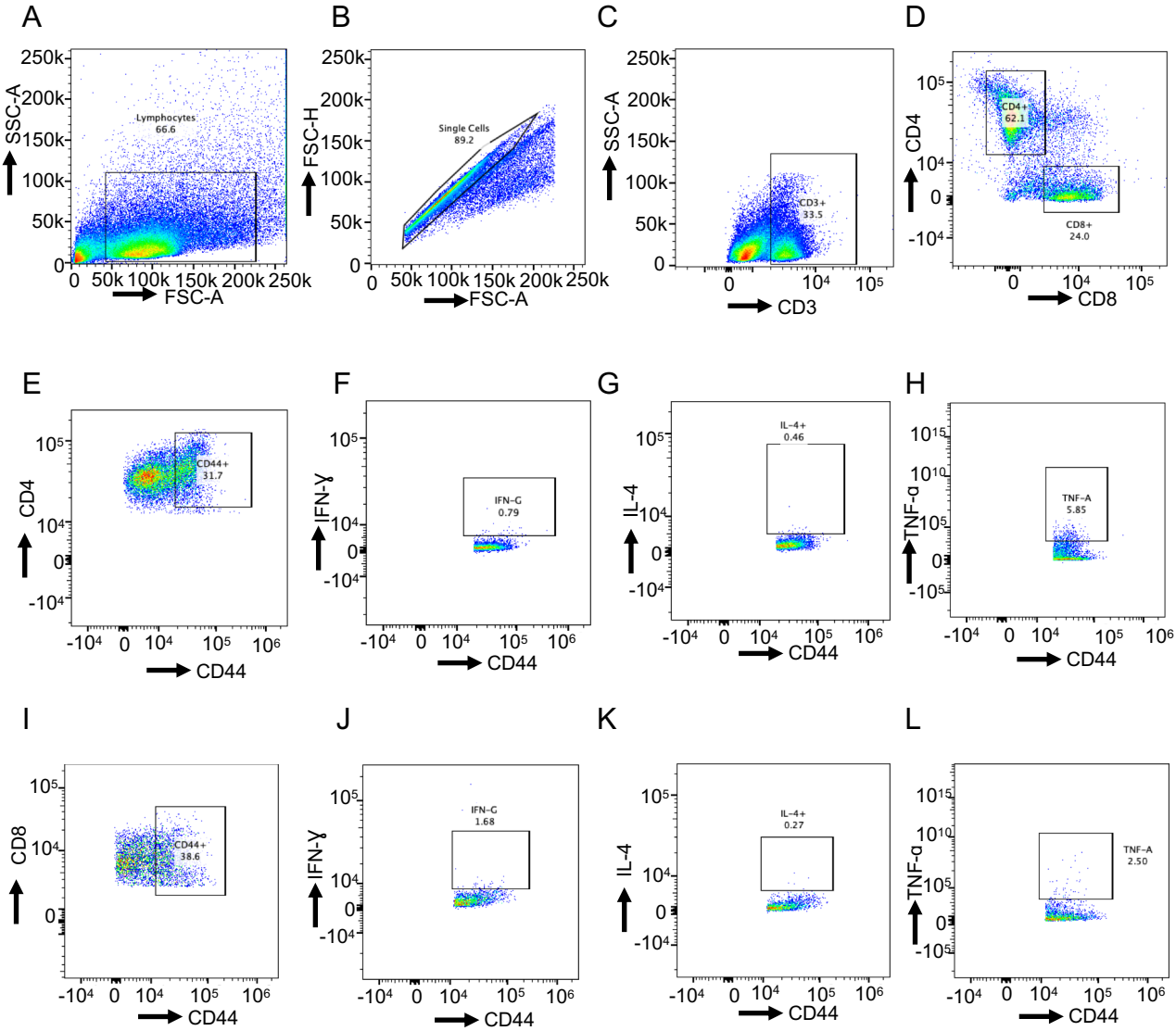
A
SSC-A
FSC-A
Lymphocytes
66.6
B
FSC-H
FSC-A
Single Cells
89.2
C
SSC-A
CD3
CD3+
33.5
D
CD4
CD8
CD4+
62.1
CD8+
24.0
E
CD4
CD44
CD44+
31.7
F
IFN-γ
CD44
IFN-G
0.79
G
IL-4
CD44
IL-4+
0.46
H
TNF-α
CD44
TNF-A
5.85
I
CD8
CD44
CD44+
38.6
J
IFN-γ
CD44
IFN-G
1.68
K
IL-4
CD44
IL-4+
0.27
L
TNF-α
CD44
TNF-A
2.50

Figure S2. Analysis of intracellular IFNγ, TNFα and IL-4 levels in the RBD peptide pool-stimulated CD4, CD8 positive T-cells derived from the splenocytes of Circ-RBD immunized mice.

(A)-(D) Representative FACS plot showing the gating strategy of lymphocytes (A), single cells (B), $CD3^+$ (C) and $CD4^+CD8^+$(D) T-cells.

(E)-(H) Representative FACS plot showing the gating strategy of $CD4^+$ memory T-cells (E) and quantification of IFNγ (F), IL-4 (G) and TNFα (H) in $CD4^+$ memory T-cells.

(I)-(L) Representative FACS plot showing the gating strategy of $CD8^+$ memory T-cell (J) and quantification of IFNγ (K), IL-4 (K) and TNFα (L) in $CD8^+$ memory T-cells.

Figure S3

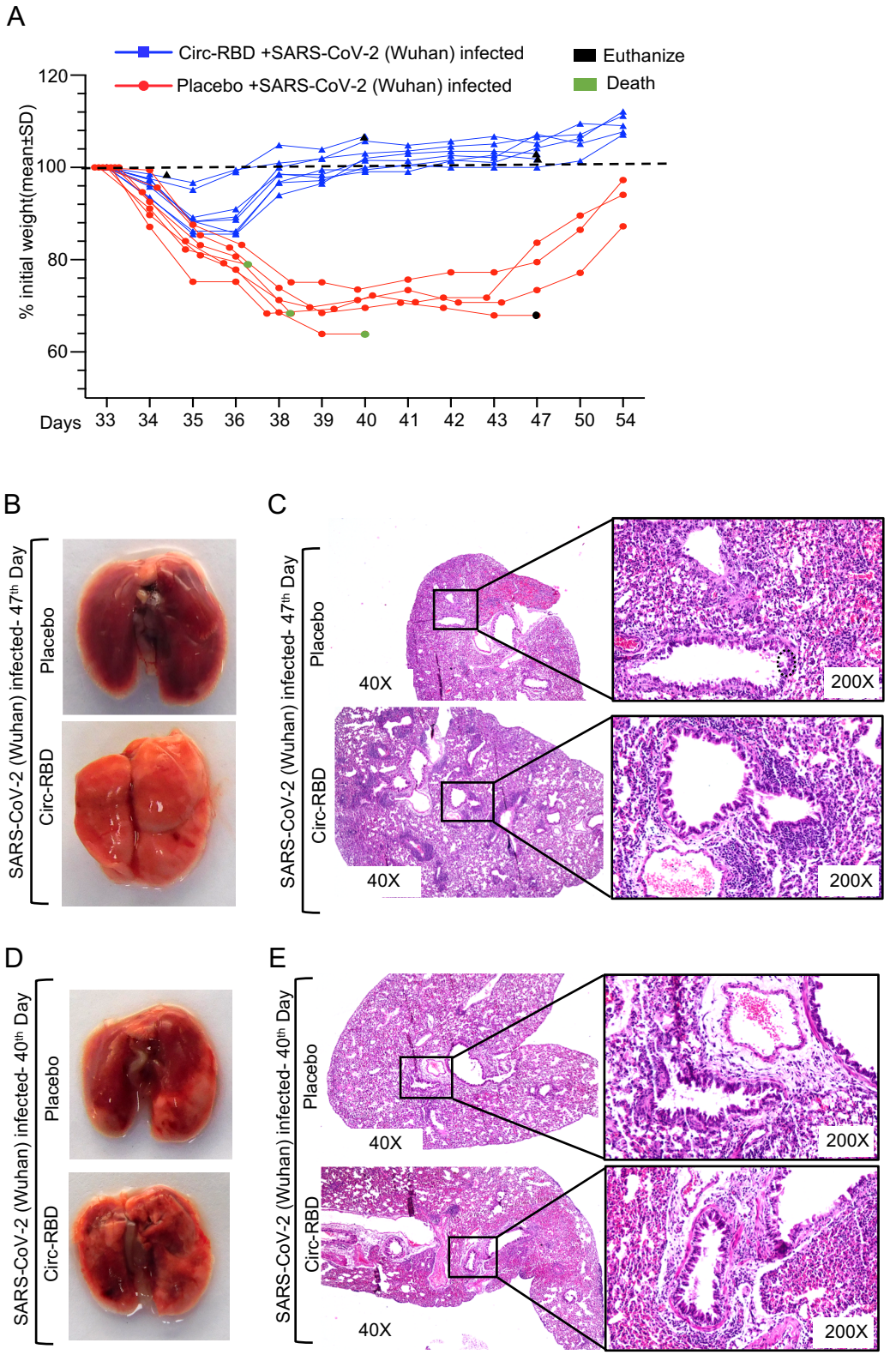
A
Circ-RBD +SARS-CoV-2 (Wuhan) infected
Placebo +SARS-CoV-2 (Wuhan) infected
Euthanize
Death
% initial weight(mean±SD)
120
100
80
60
Days
33
34
35
36
38
39
40
41
42
43
47
50
54
B
SARS-CoV-2 (Wuhan) infected- 47th Day
Placebo
Circ-RBD
C
SARS-CoV-2 (Wuhan) infected- 47th Day
Placebo
Circ-RBD
40X
200X
40X
200X
D
SARS-CoV-2 (Wuhan) infected- 40th Day
Placebo
Circ-RBD
E
SARS-CoV-2 (Wuhan) infected- 40th Day
Placebo
Circ-RBD
40X
200X
40X
200X

1399 **Figure S3. Immunization with the Circ-RBD protects mice from intra-tracheal SARS-**
1400 **CoV-2 challenge.**
1401 (A) Effect of the SARS-CoV-2 (Wuhan) infection on mice weight. Weight of each mouse in the
1402 placebo and the Circ-RBD immunization group was measured (initial no. of mice in both
1403 groups = 7) on the indicated days between day 33 to day 54 and the percent weight change
1404 with respect to the weight on day 33 (considered 100%) is plotted in the graph. Few animals
1405 in the placebo group died during the experimental period.
1406 (B) Lung morphology of the placebo and Circ-RBD immunized, SARS-CoV-2 (Wuhan)
1407 infected mice, collected on day 47.
1408 (C) Representative hematoxylin and eosin-stained image of lung tissue section prepared from
1409 the placebo and Circ-RBD immunized, SARS-CoV-2 (Wuhan) infected mice, collected on day
1410 47. Images were acquired at 40X (left panel) and 200X magnification (right panel).
1411 (D) Lung morphology of the placebo and Circ-RBD immunized, SARS-CoV-2 (Wuhan)
1412 infected mice, collected on day 40.
1413 (E) Representative hematoxylin and eosin-stained image of lung tissue section prepared from
1414 the placebo and Circ-RBD immunized, SARS-CoV-2 (Wuhan) infected mice, collected on day
1415 40. Images were acquired at 40X (left panel) and 200X magnification (right panel).